



## Similarities and differences in affinity and binding modes of tricyclic pyrimido- and pyrazinoxanthines at human and rat adenosine receptors



Ewa Szymańska<sup>a</sup>, Anna Drabczyńska<sup>a</sup>, Tadeusz Karcz<sup>a</sup>, Christa E. Müller<sup>b</sup>, Meryem Köse<sup>b</sup>, Janina Karolak-Wojciechowska<sup>c</sup>, Andrzej Fruziński<sup>c</sup>, Jakub Schabikowski<sup>a</sup>, Agata Doroz-Płonka<sup>a</sup>, Jadwiga Handzlik<sup>a</sup>, Katarzyna Kieć-Kononowicz<sup>a,\*</sup>

<sup>a</sup> Department of Technology and Biotechnology of Drugs Jagiellonian University Medical College, Medyczna 9, PL 30-688 Kraków, Poland

<sup>b</sup> PharmaCenter Bonn, Pharmaceutical Institute, Pharmaceutical Chemistry I, University of Bonn, An der Immenburg 4, 53121 Bonn, Germany

<sup>c</sup> Institute of General and Ecological Chemistry, Technical University of Łódź, Żwirki 36, 90-924 Łódź, Poland

### ARTICLE INFO

#### Article history:

Received 31 March 2016

Revised 9 July 2016

Accepted 15 July 2016

Available online 18 July 2016

#### Keywords:

Adenosine receptor

Docking

Homology modeling

Purine-2,6-dione

Species differences

Subtype selectivity

Xanthines

### ABSTRACT

A new series of 32 pyrimido- and 5 tetrahydropyrazino[2,1-*f*]purinediones was obtained and evaluated for their adenosine receptors (ARs) affinities. The 1,3-dibutyl derivative of 9-(4-(2-(dimethylamino)ethoxy)phenyl)-6,7,8,9-tetrahydropyrimido[1,2-*f*]purine-2,4(1*H*,3*H*)-dione was found to be the most potent A<sub>1</sub> AR antagonist of the present series, showing selectivity over the other AR subtypes. The structure–activity for the obtained purinediones was established. Docking experiments of the investigated library to homology models of the human and rat A<sub>1</sub> and A<sub>2A</sub> ARs allowed to compare the expected binding modes for selected compounds. The detailed analysis of binding cavities within individual AR subtypes indicated small but significant structural variations that may underlie the observed differences in binding affinities of purinediones at particular subtypes and species.

© 2016 Published by Elsevier Ltd.

### 1. Introduction

Methylxanthines, including caffeine, theobromine and theophylline, occur naturally in a number of species of plants belonging to 28 genera and over 17 families, but the most common sources are coffee, tea and cacao.<sup>1</sup> The history of the medicinal use of cacao, both as a primary remedy and as a vehicle to deliver other medicines, dates back to the Olmecs, the first elaborate pre-Columbian civilization of Mesoamerica (1200–400 BCE), where a beverage made from of *Theobroma cacao* beans ‘Xocolatl’ was highly valued for its stimulating effect and healing properties.<sup>2</sup> Nowadays methylxanthines, therapeutically used as bronchodilators and for other indications, are probably the most widely self-administered psychostimulatory drugs in the world.<sup>1</sup> Natural xanthines (e.g. caffeine **1**, Fig. 1A) and their synthetic derivatives exhibit a variety of physiological effects, such as positive inotropic and chronotropic effects on the heart, decreased airway resistance in the lung and respiratory tract, stimulation as well as significant behavioral

effects on measures of locomotor activity, schedule-controlled behavior, drug self-administration, and learning and memory. Most of these effects are likely due to the non-selective inhibition of adenosine receptors.<sup>3–5</sup>

Adenosine, an endogenous purine nucleoside, acts as a neuro-modulator in both the central and peripheral nervous systems by interacting with the P1 group of purine receptors, belonging to the class A family of G protein-coupled receptors (GPCR). Four adenosine receptor (AR) subtypes, A<sub>1</sub>, A<sub>2A</sub>, A<sub>2B</sub> and A<sub>3</sub>, are known and have been pharmacologically characterized. Activation of the A<sub>1</sub> and A<sub>3</sub> receptors inhibits the production of cyclic AMP via G<sub>i/o</sub> protein, while A<sub>2A</sub> and A<sub>2B</sub> receptor activation stimulates the activity of the adenylate cyclase via G<sub>s</sub> protein, inducing an increase in cAMP levels.<sup>6</sup>

The therapeutic potential of adenosine receptors ligands depends on the diverse distribution of ARs throughout the body, both in the central nervous system (CNS) and in peripheral tissues. Thus, subtype-selective AR antagonists have been of interest as potential kidney-protective (A<sub>1</sub> AR), antifibrotic (A<sub>2A</sub> AR), neuro-protective (A<sub>2A</sub> AR), antiasthmatic (A<sub>2B</sub> AR), antiglaucoma (A<sub>3</sub> AR), and anti-cancer (A<sub>2A</sub>, A<sub>2B</sub>) drugs.<sup>3,7–10</sup> The A<sub>1</sub> AR-selective

\* Corresponding author. Tel.: +48 012 620 55 80; fax: +48 012 620 55 96.

E-mail address: [mfkonono@cyf-kr.edu.pl](mailto:mfkonono@cyf-kr.edu.pl) (K. Kieć-Kononowicz).

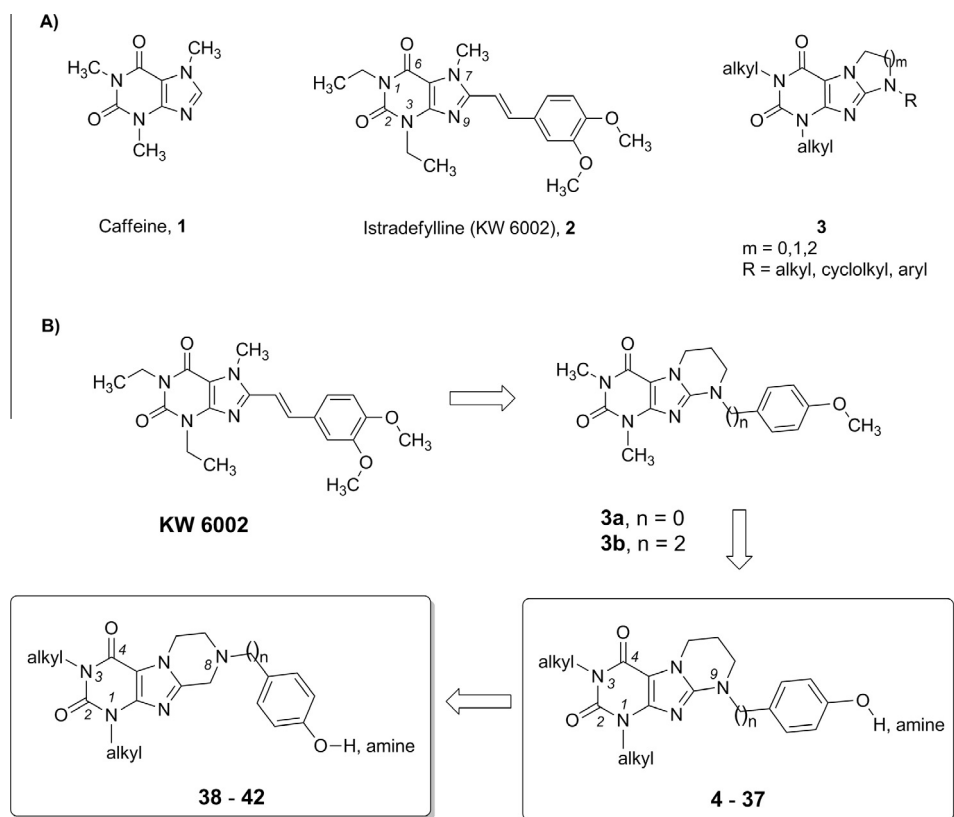


**Figure 1.** (A) Structures of xanthine-based antagonists of adenosine receptors. (B) Scheme of structural modifications within the current study. Please note that according to the IUPAC system the numbering of atoms for tricyclic compounds is different than for bicyclic xanthine derivatives.

xanthine-derived antagonists tonapofylline and rolofylline have been explored for clinical applications in heart failure, for improving renal function and for the treatment of acute renal failure.<sup>11,12</sup> Among the  $A_{2A}$  AR antagonists, the xanthine-based istradefylline (2, Fig. 1A) has been evaluated in clinical trials for Parkinson's disease (PD) and depression and has been recently approved in Japan as an antiparkinsonian drug.<sup>13</sup> The blockade of  $A_{2A}$  ARs localized in the brain has been proposed not only for the treatment of motor deficits in PD, but also for Alzheimer's disease and Huntington's disease.<sup>14–17</sup>

The structure–activity relationships (SAR) of xanthine-derived AR antagonists, including polycyclic fused ring systems, at various adenosine receptors subtypes has been intensively studied by our groups as well as others.<sup>18–24</sup> In general, modification of the xanthine scaffold at the 8-position with aryl, alkylaryl or cycloalkyl groups increases affinity at the  $A_1$  AR or may result in high affinity for  $A_{2B}$  AR. Introducing an alkene spacer into this position connected to an aromatic ring, e.g., the styryl residue, typically leads to increased potency and selectivity for the  $A_{2A}$  AR (e.g., KW6002).<sup>24–26</sup> A separate class of xanthines with modified 8-position is represented by tricyclic compounds containing a third ring fused to the *f*-bond of the 2,6-purinedione system. As previously reported by our groups, tricyclic dihydroimidazo-, tetrahydropyrimido- and tetrahydrodiazepino[1,2-*f*]purinediones can act as relatively potent  $A_{2A}$  AR (or  $A_{2A}/A_1$  AR) antagonists, in which the annelated pyrimidine ring appears to be beneficial for activity (3, Fig. 1A).<sup>18–22</sup> From a structural point of view, these compounds can be treated as sterically fixed and configurationally stable analogs of (*E*)-8-styrylxanthines, the scaffold that is contributing to the high  $A_{2A}$  AR affinity of istradefylline. Unfortunately, the drawback of this class of xanthine derivatives is their low water-solubility leading to poor bioavailability.<sup>24</sup>

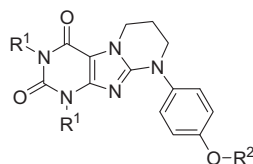
In the present project we focused on a new series of tricyclic 9-aryl/arylethyl-tetrahydropyrimido[1,2-*f*]purine-2,4-diones. As a starting point for modifications two previously described compounds were chosen, with their constrained structure mimicking the structure of (*E*)-8-styrylxanthines previously developed as  $A_{2A}$  AR ligands (Fig. 1B): 3a ( $A_{2A}$  AR antagonist)<sup>18</sup> and 3b (dual  $A_{2A}$  and  $A_1$  AR antagonist).<sup>19</sup> The primary goal of this work was to increase the affinity and selectivity for either  $A_{2A}$  or  $A_1$  ARs and to overcome the problem of low solubility.

For these purposes the following structural changes have been introduced:

- (1) In addition to the two previously reported hydroxyphenyl derivatives 4 and 8 included in this paper as reference compounds,<sup>18,19</sup> six new 4-hydroxyphenyl compounds were synthesized and evaluated (Tables 1–3);
- (2) An aliphatic tertiary amino group which increases the basicity and solubility of the parent compound has been introduced at the alkoxy chain attached to the benzene ring. Dimethylamine, diethylamine, pyrrolidine, piperidine and morpholine derivatives were prepared (Tables 1 and 2);
- (3) The tetrahydropyrimidine ring was replaced by a tetrahydropyrazine ring; this regioisomeric change shifts the *N*-arylalkylamino substituent from the 9- to the 8-position (Table 3). The N8 nitrogen atom is expected to exhibit increased basicity due to its increased aliphatic character, compared to the N9 atom.<sup>27</sup>

For all synthesized tricyclic xanthines their affinity to native rat  $A_1$  ( $rA_1$ ) ARs and  $A_{2A}$  ( $rA_{2A}$ ) ARs as well as to human recombinant  $A_{2B}$  ( $hA_{2B}$ ) ARs and  $A_3$  ( $hA_3$ ) ARs was determined in radioligand binding assays. Selected compounds were further evaluated for

**Table 1**  
Affinities of N9-aryl-tetrahydropyrimido[2,1-f]purinediones at A<sub>1</sub>–A<sub>3</sub> adenosine receptors



Compd	R <sup>2</sup>	QPlog P <sub>o/w</sub> <sup>*</sup>	QPlog S <sup>*</sup>	K <sub>i</sub> ± SEM [nM] (% inh. ± SEM at 1 μM)							
				rA <sub>1</sub> [ <sup>3</sup> H]CCPA	rA <sub>2A</sub> [ <sup>3</sup> H]MSX-2	rA <sub>2B</sub> [ <sup>3</sup> H]PSB-603	rA <sub>3</sub> [ <sup>3</sup> H]NECA	hA <sub>1</sub> [ <sup>3</sup> H]CCPA	hA <sub>2A</sub> [ <sup>3</sup> H]MSX-2	hA <sub>2B</sub> [ <sup>3</sup> H]PSB-603	hA <sub>3</sub> [ <sup>3</sup> H]PSB-11
<i>R</i> <sup>1</sup> = methyl											
<b>3a</b> <sup>18</sup>	–CH <sub>3</sub>	2.741	–4.244	>25,000 (29 ± 3) <sup>a</sup>	998 ± 70 (94 ± 6) <sup>a</sup>	nd	nd	nd	nd	nd	nd
<b>4</b> <sup>18</sup>	–H	2.209	–4.453	35,000 ± 2000 (42) <sup>a</sup>	1620 ± 310	nd	nd	nd	nd	>1000 (5 ± 5)	>>1000 (6 ± 3)
<b>12</b>		2.029	–1.589	>1000 (2 ± 2)	>>1000 (3 ± 8)	nd	nd	nd	nd	>1000 (1 ± 6)	>>1000 (–1 ± 5)
<b>13</b>		2.587	–1.830	>1000 (–3 ± 3)	>>1000 (12 ± 10)	nd	nd	nd	nd	>1000 (–5 ± 2)	>>1000 (3 ± 5)
<b>14</b>		2.469	–2.006	>1000 (3 ± 3)	>>1000 (13 ± 5)	nd	nd	nd	nd	>1000 (3 ± 3)	>>1000 (0 ± 5)
<b>15</b>		2.631	–2.237	>1000 (0 ± 1)	>>1000 (–4 ± 9)	nd	nd	nd	nd	>1000 (–1 ± 3)	>>1000 (6 ± 8)
<b>16</b>		1.597 2.278 <sup>**</sup>	–1.072 –3.271 <sup>**</sup>	>1000 (–1 ± 4)	>>1000 (14 ± 7)	nd	nd	nd	nd	>1000 (–7 ± 3)	>>1000 (–5 ± 4)
<i>R</i> <sup>1</sup> = ethyl											
<b>5</b>	–H	3.014	–4.986	>1000 (14 ± 2)	893 ± 97 (53 ± 2)	nd	nd	nd	nd	>1000 (34 ± 9)	>>1000 (1 ± 2)
<b>17</b>		2.830	–2.090	297 ± 32 (36 ± 2)	>1000 (27 ± 4)	nd	nd	nd	nd	>1000 (29 ± 4)	>>1000 (–1 ± 7)
<i>R</i> <sup>1</sup> = n-propyl											
<b>6</b>	–H	3.749	–5.717	>500 (25 ± 3)	785 ± 253 (53 ± 8)	nd	nd	nd	nd	>1000 (20 ± 9)	>>1000 (18 ± 2)
<b>18</b>		3.473	–2.522	180 ± 22 (47 ± 3)	>1000 (44 ± 7)	nd	nd	nd	nd	>1000 (17 ± 2)	>>1000 (17 ± 5)
<b>19</b>		4.128	–3.178	567 ± 106 (30 ± 3)	1790 ± 510 (51 ± 7)	nd	nd	nd	nd	>1000 (22 ± 7)	>1000 (20 ± 3)
<b>20</b>		4.011	–3.342	175 ± 44 (53 ± 5)	>1000 (28 ± 4)	>1000 (4 ± 2)	>1000 (10 ± 9)	1990 ± 140 (22 ± 3)	2380 ± 450 (29 ± 6)	>1000 (10 ± 4)	>1000 (20 ± 3)
<b>21</b>		4.177	–3.470	254 ± 24 (44 ± 3)	>1000 (44 ± 5)	nd	nd	nd	nd	>1000 (18 ± 6)	>1000 (29 ± 4)
<b>22</b>		3.128 3.896 <sup>**</sup>	–1.932 –4.739 <sup>**</sup>	>1000 (14 ± 2)	1930 ± 460 (45 ± 5)	nd	nd	nd	nd	>1000 (3 ± 3)	>1000 (23 ± 3)
<i>R</i> <sup>1</sup> = n-butyl											
<b>7</b>	–H	4.501	–6.524	174 ± 19 (48 ± 1)	738 ± 141 (64 ± 3)	nd	nd	nd	nd	>1000 (33 ± 7)	>1000 (40 ± 4)
<b>23</b>		4.185	–3.196	56 ± 8 (72 ± 2)	1050 ± 90 (47 ± 2)	>1000 (9 ± 4)	>1000 (15 ± 8)	539 ± 74 (43 ± 5)	1030 ± 130 (52 ± 1)	>500 (40 ± 5)	>1000 (38 ± 8)
<b>24</b>		4.802	–3.650	137 ± 9 (55 ± 2)	1460 ± 250 (49 ± 6)	>1000 (6 ± 3)	>1000 (16 ± 7)	1190 ± 130 (30 ± 5)	1010 ± 180 (54 ± 4)	>1000 (33 ± 5)	>1000 (44 ± 2)
<b>25</b>		4.793	–4.208	72 ± 8 (69 ± 1)	989 ± 200 (49 ± 4)	>1000 (15 ± 1)	>1000 (20 ± 4)	658 ± 69 (41 ± 5)	666 ± 128 (68 ± 2)	>1000 (34 ± 1)	813 ± 140 (48 ± 2)
<b>26</b>		4.927	–4.307	127 ± 25 (65 ± 3)	1480 ± 170 (49 ± 8)	>1000 (9 ± 11)	>1000 (20 ± 2)	713 ± 119 (42 ± 4)	921 ± 29 (53 ± 4)	>500 (41 ± 2)	854 ± 69 (48 ± 2)
<b>27</b>		3.912 4.318 <sup>**</sup>	–2.683 –4.128 <sup>**</sup>	268 ± 14 (35 ± 2)	>1000 (31 ± 2)	nd	nd	nd	nd	>1000 (27 ± 8)	>1000 (38 ± 5)

nd—not determined.

<sup>a</sup> Tested at 25 μM.

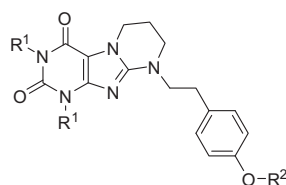
<sup>\*</sup> Protonated form (charge +1).

<sup>\*\*</sup> Not protonated (neutral) form.

their affinity to recombinant human A<sub>1</sub> (hA<sub>1</sub>)ARs, human A<sub>2A</sub> (hA<sub>2A</sub>)ARs, rat (rA<sub>2B</sub>) A<sub>2B</sub> ARs, and rat A<sub>3</sub> (rA<sub>3</sub>) ARs. Additionally, antagonistic properties of selected tricyclic xanthines were

examined in cAMP accumulation assay. The solubility of the synthesized series (QPlogS) was estimated by in silico calculation, and determined experimentally for selected analogues as well as

**Table 2**  
Affinities of N9-arylethyl-tetrahydropyrimido[2,1-f]purinediones at A<sub>1</sub>–A<sub>3</sub> adenosine receptors



Compd	R <sup>2</sup>	QPlogP <sub>o/w</sub> <sup>*</sup>	QPlogS <sup>*</sup>	<i>K<sub>i</sub></i> ± SEM [nM] (% inh. ± SEM at 1 μM)								
				rA <sub>1</sub> [ <sup>3</sup> H]CCPA	rA <sub>2A</sub> [ <sup>3</sup> H]MSX-2	rA <sub>2B</sub> [ <sup>3</sup> H]PSB-603	rA <sub>3</sub> [ <sup>3</sup> H]NECA	hA <sub>1</sub> [ <sup>3</sup> H]CCPA	hA <sub>2A</sub> [ <sup>3</sup> H]MSX-2	hA <sub>2B</sub> [ <sup>3</sup> H]PSB-603	hA <sub>3</sub> [ <sup>3</sup> H]PSB-11	
<i>R</i> <sup>1</sup> = methyl												
<b>3b</b> <sup>19</sup>	–CH <sub>3</sub>	2.868	–2.763	3850 ± 430	370 ± 20	nd	nd	nd	nd	nd	nd	nd
<b>8</b> <sup>19</sup>	–H	2.672	–3.554	ca. 25,000 (46) <sup>a</sup>	230 ± 10	nd	nd	>25,000 (34) <sup>a</sup>	630 ± 350	7200 ± 600 <sup>b</sup>	>10,000 (9) <sup>c</sup>	>10,000 (9) <sup>c</sup>
<b>28</b>		2.597	–1.074	>1000 (–2 ± 3)	653 ± 84 (49 ± 3)	nd	nd	nd	nd	>1000 (9 ± 4)	>>1000 (–5 ± 7)	>>1000 (–5 ± 7)
<b>29</b>		3.137	–1.426	>1000 (4 ± 2)	339 ± 48 (53 ± 4)	>1000 (–2 ± 5)	>1000 (6 ± 3)	>1000 (1 ± 4)	559 ± 89 (57 ± 4)	>1000 (6 ± 3)	>>1000 (–3 ± 4)	>>1000 (–3 ± 4)
<b>30</b>		2.995	–1.535	>1000 (7 ± 2)	>1000 (34 ± 11)	nd	nd	nd	nd	>1000 (13 ± 6)	>>1000 (3 ± 4)	>>1000 (3 ± 4)
<b>31</b>		3.301	–2.039	>1000 (3 ± 1)	645 ± 244 (65 ± 5)	nd	nd	nd	nd	>1000 (2 ± 4)	>>1000 (1 ± 7)	>>1000 (1 ± 7)
<b>32</b>		2.232 2.306 <sup>**</sup>	–0.549 –0.932 <sup>**</sup>	>1000 (0 ± 1)	585 ± 150 (71 ± 6)	nd	nd	nd	nd	>1000 (–5 ± 2)	>>1000 (–3 ± 3)	>>1000 (–3 ± 3)
<i>R</i> <sup>1</sup> = ethyl												
<b>9</b>	–H	3.350	–3.807	>1000 (14 ± 2)	271 ± 16 (80 ± 2)	>1000 (14 ± 1)	>1000 (19 ± 4)	2020 ± 70 (20 ± 3)	2180 ± 390 (30 ± 5)	>500 (42 ± 3)	>>1000 (6 ± 4)	>>1000 (6 ± 4)
<b>33</b>		2.817 2.803 <sup>**</sup>	–0.870 –0.888 <sup>**</sup>	>1000 (17 ± 2)	859 ± 23 (51 ± 2)	nd	nd	nd	nd	>1000 (36 ± 9)	>>1000 (7 ± 3)	>>1000 (7 ± 3)
<i>R</i> <sup>1</sup> = n-propyl												
<b>10</b>	–H	4.183	–5.516	370 ± 37 (33 ± 2)	464 ± 66 (67 ± 1)	nd	nd	nd	nd	663 ± 130 (58 ± 4)	>1000 (24 ± 2)	>1000 (24 ± 2)
<b>34</b>		4.526	–2.312	347 ± 33 (31 ± 1)	658 ± 115 (65 ± 3)	nd	nd	nd	nd	338 ± 14 (66 ± 4)	633 ± 52 (53 ± 3)	633 ± 52 (53 ± 3)
<b>35</b>		3.440 3.576 <sup>**</sup>	–1.287 –1.800 <sup>**</sup>	>500 (26 ± 3)	>1000 (44 ± 1)	nd	nd	nd	nd	853 ± 73 (50 ± 2)	>1000 (20 ± 4)	>1000 (20 ± 4)
<i>R</i> <sup>1</sup> = n-butyl												
<b>11</b>	–H	4.812	–5.379	184 ± 57 (51 ± 3)	518 ± 79 (63 ± 5)	nd	nd	nd	nd	131 ± 22 (80 ± 2)	619 ± 110 (44 ± 4)	619 ± 110 (44 ± 4)
<b>36</b>		5.216	–2.931	80 ± 5 (69 ± 2)	566 ± 43 (64 ± 2)	1100 ± 100 (38 ± 3)	>1000 (15 ± 3)	1550 ± 180 (27 ± 3)	546 ± 67 (64 ± 4)	109 ± 11 (87 ± 1)	310 ± 48 (75 ± 2)	310 ± 48 (75 ± 2)
<b>37</b>		4.143 4.161 <sup>**</sup>	–1.689 –2.029 <sup>**</sup>	172 ± 35 (47 ± 3)	1370 ± 270 (47 ± 5)	nd	nd	nd	nd	337 ± 79 (62 ± 4)	890 ± 84 (48 ± 5)	890 ± 84 (48 ± 5)

nd – not determined.

<sup>a</sup> Tested at 25 μM.

<sup>b</sup> Tested versus [<sup>3</sup>H]ZM241385.

<sup>c</sup> Tested at 10 μM.

<sup>\*</sup> Protonated form (charge +1).

<sup>\*\*</sup> Not protonated (neutral) form.

two lead structures. To rationalize the observed subtype selectivity as well as the species selectivity of the new compounds, molecular modeling and docking studies using homology models of both human and rat adenosine receptors were performed.

## 2. Results and discussion

### 2.1. Chemistry

The general procedure for the synthesis of the target series is outlined in Schemes 1 and 2. A several-step procedure, starting from 1,3-diethyl/1,3-dipropyl urea and cyanoacetic acid (1,3-dimethyl- and 1,3-dibutyltheophylline are commercially available)

(Scheme 1) or 1,3-dimethyl urea and cyanoacetic acid (Scheme 2) was applied using modifications of literature methods<sup>18–21</sup> to yield the key dihalogen intermediates. Formation of the tetrahydropyrimidine ring in **5–7**, **9–11** was achieved by cyclization of 8-bromo-7-(3-chloropropyl)-1,3-dialkylpurinediones with either 4-aminophenol or tyramine, in analogy to the preparation of the previously reported compounds **4** and **8**.<sup>18,19</sup> Phenol **38** was prepared by a similar cyclization reaction of 7-(2-chloroethyl)-8-(chloromethyl)-1,3-dimethyl-purinedione.

To access the library of the target ethers **12–37** and **39–42**, the corresponding phenols were refluxed with commercial 2-chloroethylamines (alkyl or heterocyclic) in 2-butanone as a solvent, in the presence of potassium carbonate as an absorbing agent of hydrogen chloride released during the reaction.

**Table 3**  
Affinities of N8-arylethyl-tetrahydropyridino[2,1-f]purinediones at A<sub>1</sub>–A<sub>3</sub> adenosine receptors

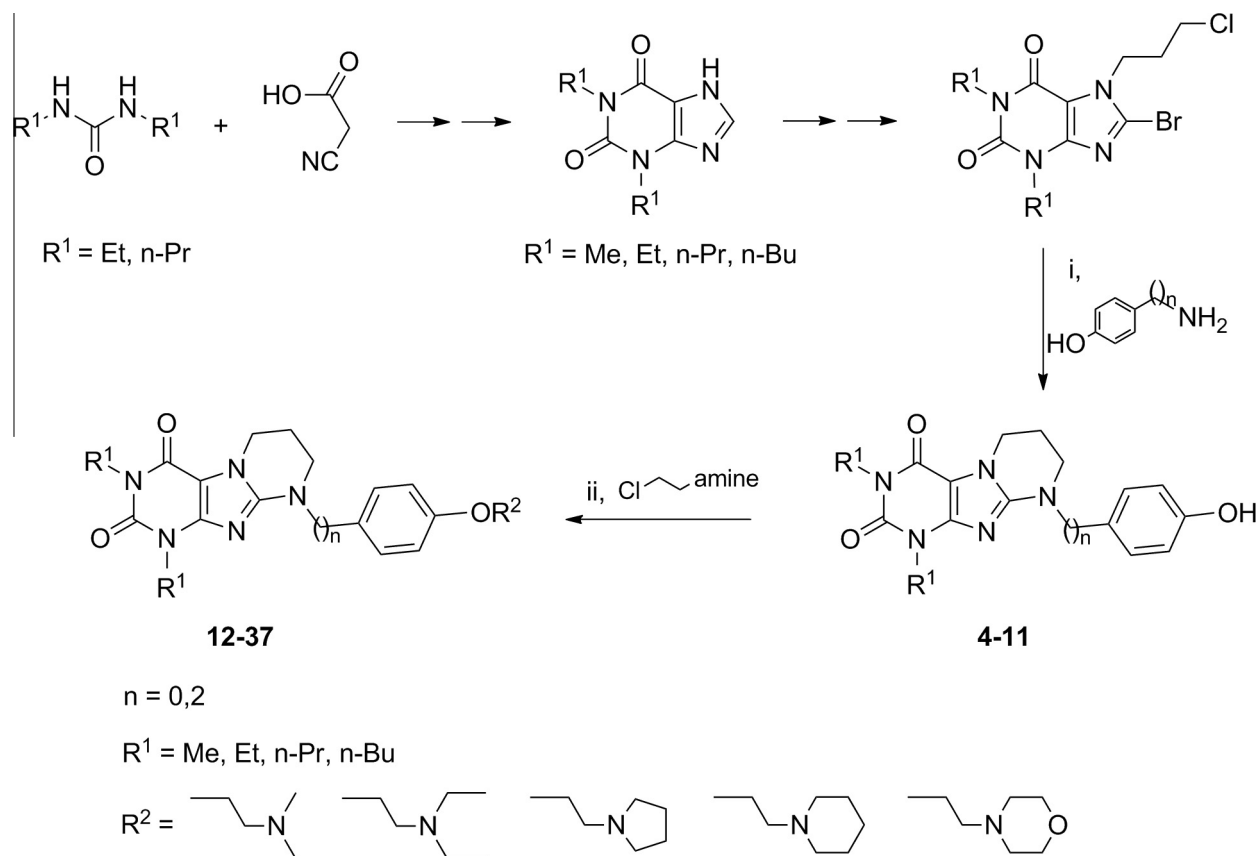
Compd	R	QPlogP <sub>o/w</sub> <sup>+</sup>	QPlogS <sup>+</sup>	rA <sub>1</sub>	rA <sub>2A</sub>	rA <sub>2B</sub>	rA <sub>3</sub>	hA <sub>1</sub>	hA <sub>2A</sub>	hA <sub>2B</sub>	hA <sub>3</sub>
				[ <sup>3</sup> H]CCPA	[ <sup>3</sup> H]MSX-2	[ <sup>3</sup> H]PSB-603	[ <sup>3</sup> H]NECA	[ <sup>3</sup> H]CCPA	[ <sup>3</sup> H]MSX-2	[ <sup>3</sup> H]PSB-603	[ <sup>3</sup> H]PSB-11
				K <sub>i</sub> ± SEM [nM] (% inh. ± SEM at 10 μM)				K <sub>i</sub> ± SEM [nM] (% inh. ± SEM at 1 μM)			
<b>38</b>	-H	1.642 1.716 <sup>**</sup>	-2.735 -3.352 <sup>**</sup>	>1000 (4 ± 2) <sup>a</sup>	>10,000 (35 ± 4)	nd	nd	nd	nd	>1000 (11 ± 7)	>1000 (3 ± 6)
<b>39</b>		1.259–1.396	0.768–1.091	1370 ± 318	6400 ± 990	nd	nd	nd	nd	>1000 (4 ± 2)	>1000 (6 ± 7)
<b>40</b>		1.761–1.884	0.634–0.901	>10,000 (42 ± 4)	7850 ± 798	nd	nd	nd	nd	>1000 (19 ± 10)	>1000 (0 ± 1)
<b>41</b>		1.934–2.055	-0.021–0.167	1740 ± 378	5640 ± 1070	nd	nd	nd	nd	>1000 (13 ± 1)	>1000 (0 ± 3)
<b>42</b>		0.961–1.007 0.936 <sup>**</sup>	0.973–1.784 1.097 <sup>**</sup>	>10,000 (22 ± 5)	11,500 ± 2650	nd	nd	nd	nd	>1000 (4 ± 3)	>1000 (3 ± 2)

nd—not determined.

<sup>a</sup> Tested at 1 μM.

<sup>+</sup> Protonated form(s) (total charge +1 or +2).

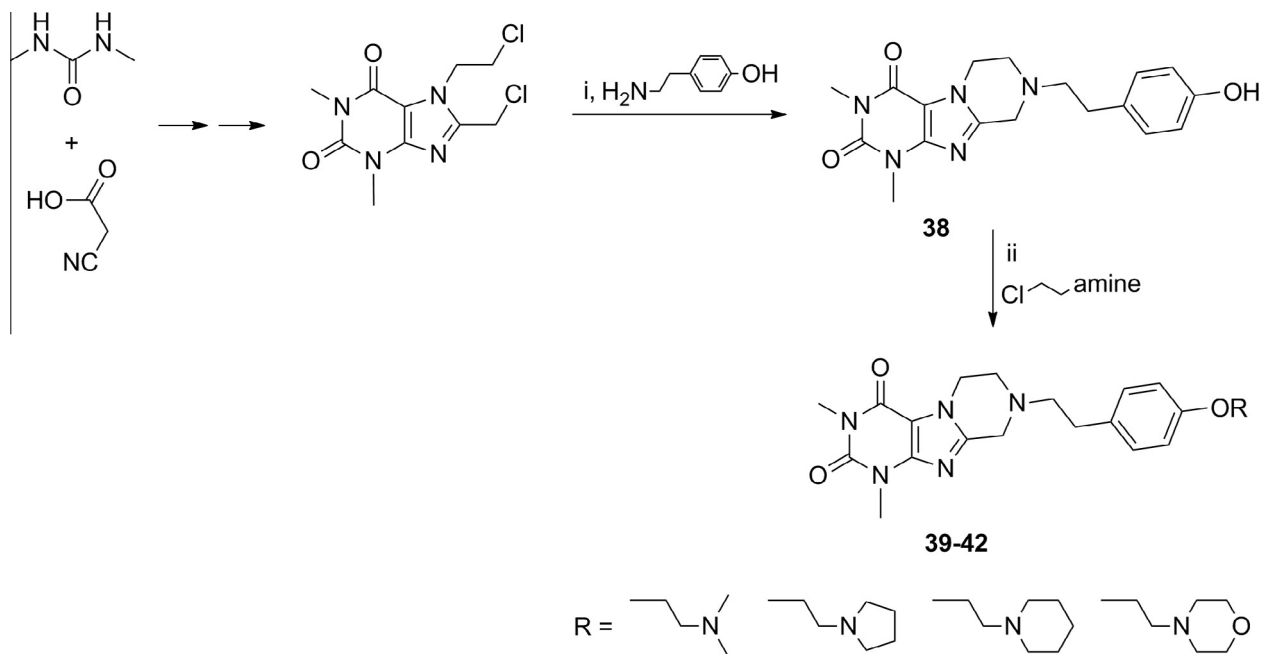
<sup>\*\*</sup> Not protonated (neutral) form.



**Scheme 1.** Synthesis of the target tetrahydropyrimido[2,1-f]purinediones. Reagents and conditions: (i) DMF; (ii) 2-butanone, K<sub>2</sub>CO<sub>3</sub>.

The structures of the obtained tricyclic xanthines were confirmed by UV, IR and NMR spectra. All compounds showed IR absorption bands typical for xanthine derivatives.<sup>28</sup> In the UV

spectra of tetrahydropyrimido[2,1-f]purinediones a bathochromic shift of a λ<sub>max</sub> value of ca. 275 nm to about 300 nm, typical for 8-aminoxanthines,<sup>29</sup> could be observed.



**Scheme 2.** Synthesis of the target tetrahydropyrazino[2,1-*f*]purinediones. Reagents and conditions: (i) DMF; (ii) 2-butanone,  $K_2CO_3$ .

## 2.2. Biological activity

### 2.2.1. Adenosine receptor affinity

The synthesized tetrahydropyrimido- and tetrahydropyrazino [2,1-*f*]purinediones were evaluated *in vitro* in radioligand binding assays for their affinity at the rat  $A_1$  and  $A_{2A}$  adenosine receptors in brain cortical membrane, and brain striatal membrane preparations, respectively. Additionally, all compounds were tested for their affinity at human recombinant  $A_{2B}$  and  $A_3$  ARs stably expressed in Chinese hamster ovary (CHO) cells. Selected tricyclic xanthines were examined at all four AR subtypes of rat and human. The following radioligands were employed:  $A_1$ : [ $^3H$ ]2-chloro-*N*6-cyclopentyladenosine ([ $^3H$ ]CCPA);  $A_{2A}$ : [ $^3H$ ]3-(3-hydroxypropyl)-7-methyl-8-(*m*-methoxystyryl)-1-propargylxanthine ([ $^3H$ ]MSX-2);  $A_{2B}$ : [ $^3H$ ]4-(2-[7-amino-2-(2-furyl)-[1,2,4]-triazolo-[2,3-*a*]-[1,3,5]-triazin-5-ylamino]ethyl)-phenol ([ $^3H$ ]ZM241385) and [ $^3H$ ]8-(4-(4-(4-chlorophenyl)piperazine-1-sulfonyl)phenyl)-1-propylxanthine ([ $^3H$ ]PSB-603);  $A_3$ : [ $^3H$ ]phenyl-8-ethyl-4-methyl-(8*R*)-4,5,7,8-tetrahydro-1*H*-imidazo[2,1-*i*]purine-5-one ([ $^3H$ ]PSB-11) and [ $^3H$ ]5'-*N*-ethylcarboxamidoadenosine ([ $^3H$ ]NECA).

### 2.2.2. Structure–activity relationships

All of the synthesized tricyclic xanthines are based on the same core structure of 1,3-dialkyl-1*H*-purine-2,6(3*H*,7*H*)-dione, however, due to differences in their substitution pattern they can be subdivided into three separate series:

- (1) tetrahydropyrimido[2,1-*f*]purinediones with *N*9-aryl substitution: **3a**, **4–7**, **12–27** (Table 1);
- (2) tetrahydropyrimido[2,1-*f*]purinediones with *N*9-arylethyl substitution: **3b**, **8–11**, **28–37** (Table 2);
- (3) tetrahydropyrazino[2,1-*f*]purinediones with *N*8-arylethyl substitution: **38–42** (Table 3).

Within the first two groups, as with other reported tetrahydropyrimido[2,1-*f*]purinediones,<sup>18–22</sup> most of the compounds show measurable affinity at  $rA_1$  and/or  $rA_{2A}$  ARs, while affinity for  $hA_{2B}$  and  $hA_3$  ARs is observed mainly within the *N*9-arylethyl series.

The effect on the  $rA_1$  AR strongly depends on the size of the alkyl substituents at the 1- and 3-positions; within both, the *N*9-aryl and the *N*9-arylethyl series: the affinity increases with increasing length of the alkyl chains. Among the most potent derivatives are the 1,3-dibutyl-substituted compounds with  $A_1$  AR affinity ( $K_i$ ) in the range of 56–268 nM, while 1,3-dipropyl derivatives bind with an affinity of 175–567 nM (except for the non-active compounds substituted with the morpholine fragment (**22**, **35** as well as the unsubstituted **6**). A similar tendency of increasing affinity with increased alkyl chain length can also be observed among the *N*9-arylethyl compounds for both, human  $A_{2B}$  and  $A_3$  ARs ( $hA_{2B}$ : 109–337 nM for 1,3-dibutyl, 338–853 nM for 1,3-dipropyl), while in case of the *N*9-aryl series, due to low affinity, this effect for  $rA_{2A}$  AR,  $hA_{2B}$  AR and  $hA_3$  AR is much less pronounced and can only be estimated. At the same time, the affinity of the *N*9-arylethyl compounds to rat  $A_{2A}$  ARs seems to drop with enlargement of the substituents at the 1- and 3-positions. All of these observations are well in agreement with previous literature data describing structure–activity relationships (SARs) for xanthine-based adenosine receptors antagonists.<sup>24</sup>

Exchange of the 4-methoxy group of the reference compounds **3a** and **3b** for a polar hydroxyl function at the benzene ring does not appear to improve solubility of the compounds (QPlogS value, Tables 1 and 2, compounds **4** and **8**). At the same time, this modification triggered only small changes in  $rA_{2A}$  AR affinity: decrease for the *N*9-phenyl ( $K_i$  = 998 nM for **3a** and 1620 nM for **4**) and a small increase for the *N*9-phenylethyl derivative ( $K_i$  = 370 nM for **3b** and 230 nM for **8**). In the latter case the introduction of a hydroxyl group also led to a total loss of affinity at the  $rA_1$  AR.

In general, most of the investigated 4-hydroxyphenyl derivatives show submicromolar affinity at  $rA_{2A}$  ARs. The  $rA_{2A}$  AR affinity within the *N*9-aryl series for **4–7** slightly increases with prolongation of the  $R^1$  alkyl chain:  $K_i$  = 1620 nM (**4**) > 893 nM (**5**) > 785 nM (**6**) > 738 nM (**7**), while among the *N*9-arylethyl compounds **8–11** this effect is inverse, and a weak drop in affinity can be observed:  $K_i$  = 230 nM (**8**) < 271 nM (**9**) < 464 nM (**10**) < 518 nM (**11**). The 1,3-dibutyl- derivative **11** is also found to be a moderately potent antagonist at the rat  $A_1$  AR and the human  $A_{2B}$  AR as well as a weak

antagonist at the A<sub>3</sub> AR with K<sub>i</sub> values of 184 nM, 131 nM and 619 nM, respectively.

Insertion of a basic amino group into the N9-substituent resulted in a significant increase in the calculated solubility of compounds. Under neutral pH conditions (pH = 7 ± 2) the tertiary aliphatic amines are protonated and form highly soluble ammonium salts, including morpholine, which is present as a mixture of a cation and the free base (for N-ethylmorpholine pK<sub>a</sub> = 7.67).<sup>30</sup> From an SAR point of view, the presence of 4-(2-aminoethoxy) fragments at the benzene ring reduces rat A<sub>2A</sub> AR affinity in both, the N9-aryl and the N9-arylethyl series to varying degrees, compared to the 4-hydroxyl compounds. Within the N9-arylethyl series the smallest reduction in rA<sub>2A</sub> AR binding affinity (in comparison with the 4-OH analogues) can be observed in case of the diethylamine: K<sub>i</sub> = 339 nM (**29**) versus 230 nM (**8**), 658 nM (**34**) versus 464 nM (**10**), 566 nM (**36**) versus 518 nM (**11**).

On the other hand, the exchange of the hydroxyl for a 4-(2-aminoethoxy) group seems to exert a strong positive influence on rat A<sub>1</sub> AR affinity, especially among the N9-aryl-substituted compounds. N,N-Dimethylamine and pyrrolidine were found to be beneficial for A<sub>1</sub> AR potency. Even in case of a small ethyl R<sup>1</sup> substituent, N,N-dimethylamine derivative **17** shows quite high potency at the rat A<sub>1</sub> AR, and with systematic enlargement of R<sup>1</sup> the affinity increases: K<sub>i</sub> = 297 nM (**17**) > 180 nM (**18**) > 56 nM (**23**). A similar tendency is seen for pyrrolidine compounds: K<sub>i</sub> = 175 nM (**20**) > 72 nM (**25**). Moderate to high affinity for the rA<sub>1</sub> AR is displayed among the 1,3-dipropyl- and 1,3-dibutyl-substituted analogues belonging to the N9-aryl or the N9-arylethyl series and containing N,N-diethylamine (**19**, **24**, **34**, **36**), piperidine (**21**, **26**) and morpholine (**27**, **37**) groups.

The most potent antagonists at the rA<sub>1</sub> AR, **23** and **25**, belonging to the N9-aryl-substituted derivatives, with K<sub>i</sub> values of 56 nM and 72 nM, respectively, display at least an 11-fold preference for rA<sub>1</sub> AR over rA<sub>2A</sub> A, hA<sub>2B</sub> A and hA<sub>3</sub> ARs. At the same time, xanthine **36**, the most potent A<sub>1</sub> AR antagonist within the N9-arylethyl series (K<sub>i</sub> = 80 nM), turned out to be less selective, showing a similarly high affinity also for the hA<sub>2B</sub> AR (K<sub>i</sub> = 109 nM) and moderate affinity for the hA<sub>3</sub> AR and the rA<sub>2A</sub> AR (K<sub>i</sub> = 310 nM and 566 nM, respectively). In general, affinity for hA<sub>2B</sub> and hA<sub>3</sub> ARs can be observed mainly (A<sub>3</sub> AR) or even exclusively (A<sub>2B</sub> AR) among the N9-arylethyl-substituted xanthine derivatives. 1,3-Dipropyl- and 1,3-dibutyl-substituted derivatives of this series are almost equipotent at rA<sub>1</sub> and hA<sub>2B</sub> ARs (while being several-fold less potent at rA<sub>2A</sub> AR and hA<sub>3</sub> AR). Thus, compounds **11** (unsubstituted hydroxyl derivative) and **36** (diethylamine) are the most potent hA<sub>2B</sub> AR ligands out of all synthesized xanthines, with K<sub>i</sub> values of 131 nM and 109 nM, respectively.

No clear correlation between affinities and the estimated solubility of the synthesized compounds has been found (Tables 1–3). Exchange of the 4-methoxy substituent in **3a** and **3b** for a 4-hydroxyl group resulted in a small drop in calculated solubility, while insertion of an amine moiety, especially a morpholine ring, into the tetrahydropyrimido[2,1-f]purinedione structure significantly increased the estimated solubility compared to **3a**, **3b**. The series of N9-arylethyl compounds generally appear to show higher solubility compared to N9-aryl tetrahydropyrimido[2,1-f]purinediones, with the most soluble one being the morpholine derivatives **32** and **33** (in the protonated form of amine). In both series, with prolongation of alkyl chains in positions 1 and 3 the solubility of compounds decreases, while in most cases their affinity for rat and human adenosine receptors increases. The most potent rA<sub>1</sub> AR antagonist **23** displays high lipophilicity (QPlogP<sub>o/w</sub> = 4.19) and a quite low predicted solubility (QPlogS = –3.20).

In addition to the series of tetrahydropyrimido[2,1-f]purinediones, several tetrahydropyrazino[2,1-f]purinediones were synthesized and investigated. The exchange of the

tetrahydropyrimidine for the tetrahydropyrazine ring was intended as a modification leading to increased water solubility. Compounds with this structure were expected to bind to A<sub>1</sub> A and/or A<sub>2A</sub> ARs.<sup>27</sup> Indeed, N8-arylethyl-substituted tetrahydropyrazino[2,1-f]purinediones containing an additional amino group (**39–42**) were predicted to show very high solubility and low lipophilicity, compared to the rest of the synthesized compounds within our library (Table 3). At the same time the rat A<sub>2A</sub> AR affinity of **39–42** is reduced by at least 8–23-fold, compared to the tetrahydropyrimidine regioisomers **28**, **29** and **30**, **31**, and completely abolished in case of the 4-hydroxyphenyl derivative **38** compared to **8**. On the other hand, the rat A<sub>1</sub> AR affinity of some amine compounds—**39** (dimethylamine) and **41** (piperidine)—increases to micromolar levels (K<sub>i</sub> = 1370 nM and 1740 nM, respectively) in comparison to the analogues **28** and **31**. Compounds **38**, **40** and **42** do not bind to rA<sub>1</sub> ARs in our assay.

None of the synthesized tetrahydropyrazino[2,1-f]purinediones shows measurable affinity for the hA<sub>2B</sub> or to hA<sub>3</sub> subtypes of ARs.

### 2.2.3. Species differences

ARs show a high percentage of amino acid sequence identity for human and rat orthologues: A<sub>1</sub> AR 95%, A<sub>2A</sub> AR 82%, A<sub>2B</sub> AR 86%, and a bit lower for A<sub>3</sub> AR: 73%.<sup>31</sup> Despite their high homology, differences in affinity between human and other species orthologues of ARs are described in the literature, and the same phenomenon was also reported for other families of GPCRs.<sup>10,27,31–34</sup> The A<sub>1</sub> AR-selective antagonist rolofylline displays a 42-fold preference for the rat over the human A<sub>1</sub> subtype (rA<sub>1</sub> AR K<sub>i</sub> = 0.19 nM, hA<sub>1</sub> AR K<sub>i</sub> = 8 nM)<sup>10,24</sup> and the non-selective AR antagonist XAC does not bind to rat A<sub>3</sub> ARs but shows a high affinity of 71 nM for the human A<sub>3</sub> subtype.<sup>24</sup>

As rat models are often employed in preclinical studies, we decided to determine the potency for the most potent compounds at the whole range of human and rat ARs in order to establish potential species differences in affinity and selectivity.

Within the present library of synthesized tricyclic xanthines, rat A<sub>1</sub> AR affinity of potent N9-aryl-substituted derivatives (K<sub>i</sub> in range of 56–175 nM) turns out to be 5–11-fold higher than at the human subtype (K<sub>i</sub> in range of 539–1990 nM). The best rA<sub>1</sub> AR ligand of the N9-arylethyl series (**36**) is over 19-fold more potent at rat than at human A<sub>1</sub> ARs (rA<sub>1</sub> K<sub>i</sub> = 80 nM, hA<sub>1</sub> K<sub>i</sub> = 1550 nM). At the same time, **36** shows a 10-fold preference for the human versus the rat A<sub>2B</sub> ARs (rA<sub>2B</sub> K<sub>i</sub> = 1100 nM, hA<sub>2B</sub> K<sub>i</sub> = 109 nM), and at least 3-fold preference for the human over the rat A<sub>3</sub> subtype (rA<sub>3</sub> K<sub>i</sub> > 1000 nM, hA<sub>3</sub> K<sub>i</sub> = 310 nM).

In case of A<sub>2A</sub> AR affinity, the N9-phenylethyl-substituted derivatives show usually higher potency at rat than at human receptors. The highest, almost 10-fold difference can be observed for 4-hydroxyphenyl compound **9**: rA<sub>2A</sub> AR K<sub>i</sub> = 271 nM, hA<sub>2A</sub> AR K<sub>i</sub> = 2180 nM. On the other hand, compounds with an N9-aryl structure show equipotency or even a weak preference at human A<sub>2A</sub> AR compared to the rA<sub>2A</sub> AR (**23–26**).

### 2.2.4. Functional assays

Our previous studies on pyrimido[2,1-f]purinediones revealed that all compounds belonging to this group displayed antagonistic properties. Nevertheless, we performed cAMP accumulation assays in CHO cells expressing human recombinant A<sub>2A</sub> AR or A<sub>2B</sub> ARs for the most active ligands in order to confirm their expected antagonistic properties. The second messenger responses to various concentrations of the non-selective agonist NECA were measured in the presence or absence of fixed concentrations of test compound. Gaddum/Schild shift analysis was performed for the obtained data to determine the K<sub>b</sub> values of the antagonists.

Two selected potent compounds were further characterized in functional assays at A<sub>2A</sub> ARs. The results obtained in cAMP accumulation assays confirmed that the compounds behave as competitive

antagonists (Figs. 2A and 2B). They cause a right-shift of the concentration–response curve for the agonist NECA, resulting in an increase of the agonist's  $EC_{50}$  value in the presence of the antagonists. Xanthine **29** at a concentration of 5  $\mu$ M changes the  $EC_{50}$  value of NECA from 68 nM to 460 nM, whereas the hydroxyl derivative **8**, used at a concentration of 7  $\mu$ M, causes a shift of the  $EC_{50}$  value of NECA from 77 nM to 302 nM. The  $K_b$  value determined for **29** in the functional assay (839 nM) is well in accordance with the  $K_i$  value determined in radioligand binding studies (559 nM). Compound **8** has been found to be somewhat weaker in the functional assay ( $K_b = 2220$  nM) than in the radioligand binding assay ( $K_i = 630$  nM), but the results are still consistent.

Similarly to the above-mentioned observations, xanthine **36**—the most potent non-selective  $A_{2B}$  AR ligand of the present work—was also classified as a competitive antagonist, according to the Gaddum/Schild  $EC_{50}$  shift analysis in cAMP accumulation assays using CHO cells stably expressing the human  $A_{2B}$  AR. Compound **36** caused an  $EC_{50}$  value shift for NECA from 73 nM to 335 nM, and the corresponding  $K_b$  value was calculated to be 547 nM (Fig. 2C).

### 2.3. Water solubility of selected compounds

The water-solubility of selected *N*9-aryl and *N*9-arylethyl substituted tetrahydropyrimido[2,1-*f*]purinediones, including two

lead structures (**3a**, **3b**) and their modifications (**19**, **23**, **29** and **36**) was determined by UV spectroscopy on the basis of the method described earlier.<sup>35</sup> Results clearly indicate that introduction of 2-aminoethoxy moiety improved water solubility within the considered series of purinediones, compared to lead compounds **3a** and **3b** possessing the methoxy group. Although all compounds displayed rather low water solubility (<1 mg/mL), the values determined for both lead structures are significantly lower than those of their modifications **19**, **23**, **29** and **36** (Table 4). The presence of a linker between *N*9 atom and the benzene ring as well as the length of alkyl chains at 1,3-positions seem to play an important role. *N*9-arylethyl compounds (**29**, **36**) demonstrated the highest solubility in this group, whereas analogues belonging to the *N*9-aryl series (**19**, **23**) showed the 3-fold lower solubility in the assay.

### 2.4. Molecular modeling

To address the observed  $A_1/A_{2A}$  AR subtype selectivity as well as species differences, docking both to the published X-ray structure of the human  $A_{2A}$  AR (PDB entry 3EML<sup>36</sup>), and to homology models of human and rat  $A_1$  and  $A_{2A}$  ARs was performed. For that we decided to use the premade homology models of ARs published by Moro and coworkers, which are freely accessible on the Adenosiland platform.<sup>37</sup>

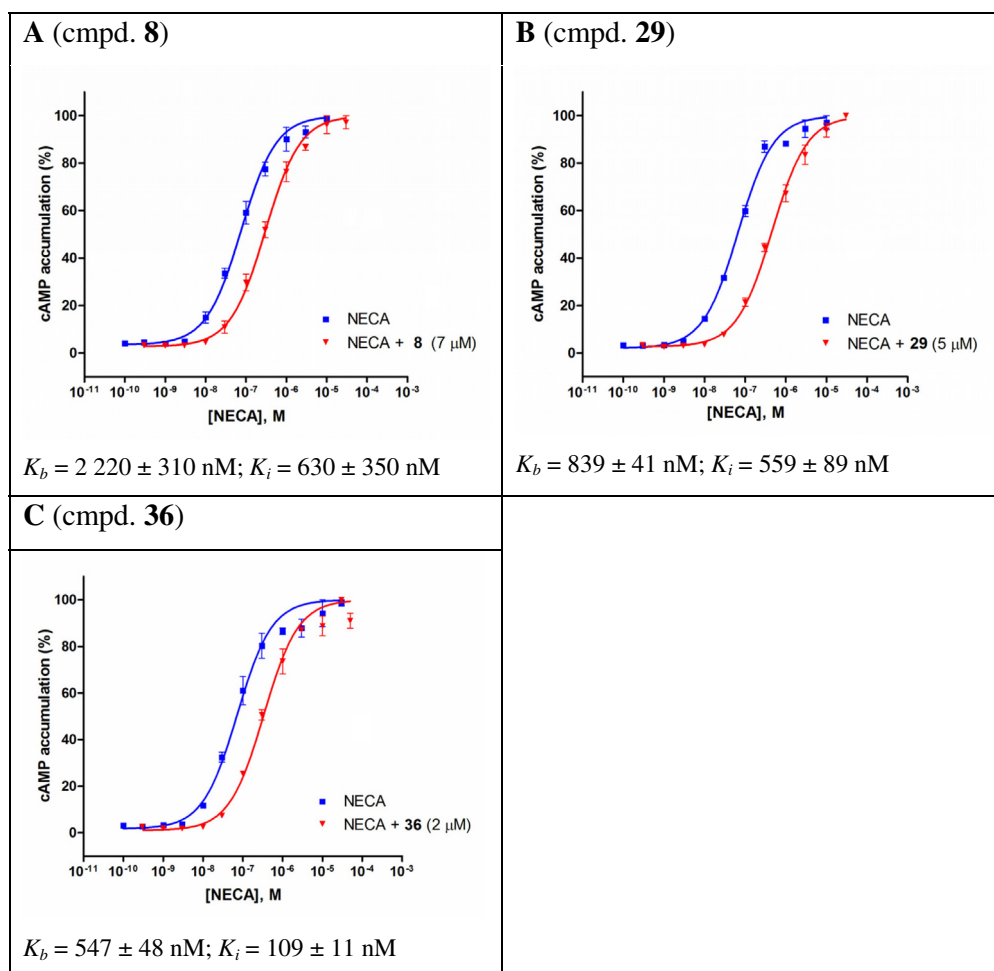


**Figure 2.** cAMP accumulation studies in CHO cells expressing the human adenosine  $A_{2A}$  (A, B) and  $A_{2B}$  (C) receptors. The dose–response curves for NECA-induced stimulation of cAMP accumulation were generated in the absence or in the presence of fixed concentrations of **8** (A), **29** (B), and **36** (C). Graphs from two independent experiments performed in duplicates with mean values  $\pm$  SEM are shown. All three investigated compounds shifted the concentration–response curve for NECA in a parallel manner to the right, indicating competitive antagonism.

**Table 4**  
Water solubility determined for selected compounds

Compound	Solubility [mg/mL]	Solubility [ $\mu$ mol/mL]
<b>3a</b>	0.051	0.150
<b>3b</b>	0.063	0.169
<b>19</b>	0.260	0.539
<b>23</b>	0.255	0.528
<b>29</b>	0.709	1.560
<b>36</b>	0.974	1.808

All the structures—the homology models of the  $hA_1$ ,  $rA_1$  and  $rA_{2A}$  AR as well as 3EML—were prepared by the same method implemented in Maestro and validated by docking in Glide.<sup>38</sup> Solvent molecules present in 3EML were deleted prior to docking. As referential set of subtype-selective, xanthine-based literature antagonists, the following compounds were used:  $A_1$  AR-selective tonapofylline and rolofylline as well as  $A_{2A}$  AR-selective istradefylline.<sup>10,24</sup> All the homology models as well as the experimental 3EML structure showed poor discrimination of the described set of AR ligands. For this reason 3EML was replaced by the 3EML-based homology model of the  $hA_{2A}$  AR,<sup>37</sup> and all four models were further optimized in a ligand-guided way by induced-fit docking<sup>38</sup> using the above-mentioned set of reference xanthines. After the validation step, the optimal, highest-ranked models were selected from the obtained clusters of AR models. Their stereochemical quality and compatibility was assessed by PROCHECK,<sup>39</sup> RAMPAGE<sup>40</sup> and ANOLEA.<sup>41</sup> Each ‘improved’ homology model together with the high-scored docking poses of the reference antagonists (rolofylline and tonapofylline for  $hA_1/rA_1$ , istradefylline for  $hA_{2A}/rA_{2A}$  ARs) were additionally analyzed in the Maestro program with respect to the model 3D structure, disulfide bonds and binding cavity.

Finally, the library of the synthesized tricyclic xanthine-based compounds was prepared. The tricyclic core of tetrahydropyrimido[2,1-f]purinedione was built, based on the reported crystallographic data for *N*9-phenyl- and *N*9-(2-benzyloxy)ethyl derivatives.<sup>18,19</sup> Models of tetrahydropyrazino[2,1-f]purinediones were constructed using the 3D information obtained from the solved X-ray structures of **38** and **42**. The ligand library was prepared with the LigPrep module (low energy ionization/protonation state at pH = 7  $\pm$  1, tautomeric state), optimized by conformational search (MacroModel) and docked using Glide SP mode with calculation of per-residue interactions.<sup>38</sup> Obtained poses were ranked according to docking scores implemented in Glide and analyzed in terms of important interactions described in the literature for each subtype of AR. According to this ranking the following docking poses were selected for further analysis: **9** at  $hA_{2A}$  AR, **9** at  $rA_{2A}$  AR, **23** at  $hA_1$  AR, **23** at  $rA_1$  AR. For detailed analysis of the binding

pocket structures, the type of residues and the position of side chains in the range of 5 Å from the docked poses of selected ligands were taken into account (Fig. 3, Ballesteros–Weinstein GPCR numbering of residues is used<sup>42–44</sup>).

To examine the ligand–protein non-bonded and polar interactions energy for each final docking pose, the overall terms of the docking score function (electrostatic interactions, van der Waals interactions and hydrogen bonding energy), as well as the energy contributions calculated for the individual residues, were analyzed.

Since the first crystal structure of the human  $A_{2A}$  AR in complex with the antagonist ZM241385 was published,<sup>36</sup> several other X-ray structures of the  $hA_{2A}$  AR, comprising agonist-bound and inactive conformations have become available. Their analysis allowed the identification of residues responsible for ligand recognition and crucial for ligand selectivity. Structural insight derived from adenosine receptor X-ray structures has also allowed for more precise molecular modeling of 3D structures of other AR subtypes.<sup>45,46</sup>

The comparison of available crystal structures of the human adenosine  $A_{2A}$  AR in complex with xanthine- and triazine-based antagonists (and inverse agonists)<sup>36,47–49</sup> allows to perceive flexibility of some amino acid side chains within the receptor binding cleft. Wide variations can be observed, e.g., in case of Glu169<sup>5,30</sup>, and Asn253<sup>6,55</sup>, two amino acids described as crucial residues for  $A_{2A}$  AR antagonist binding (residue numbering as for the human  $A_{2A}$  AR sequence P29274,<sup>50</sup> in superscript Ballesteros–Weinstein GPCR numbering, extended for extracellular loops<sup>36,42–44</sup>). In the structures of  $hA_{2A}$  AR with bound xanthine derivatives, XAC and caffeine (PDB entries 3REY and 3RFM, respectively), the Glu169<sup>5,30</sup> side chain does not form a polar interaction with a ligand, like in case of the triazine-based ligands, and adopts a rotated conformation compared to the 3EML structure.<sup>36</sup> The side chain of Asn253<sup>6,55</sup> in 3REY has a reversed position compared to other structures including 3RFM. Nevertheless, in both xanthine-bound crystal structures the ligands share a common binding mode, with the same carbonyl group (in the 6-position of a bicyclic purinedione core) forming an H-bond contact with the terminal amino group of Asn253<sup>6,55</sup>. In our calculations the observed binding system of tricyclic core resembles the canonical way of binding reported for XAC and caffeine, with the H-bond between the conserved Asn<sup>6,55</sup> and the ligand carbonyl group in the 4-position (corresponding to C=O in the 6-position of bicyclic 2,6-purinediones).

### 2.4.1. Binding mode of the xanthine **9** at the human and rat $A_{2A}$ AR models

Comparison of the observed docking poses for the  $hA_{2A}$  and the  $rA_{2A}$  ARs is illustrated with the compound **9**, a potent  $rA_{2A}$  AR antagonist showing 10-fold selectivity over the  $hA_{2A}$  AR. In case of the  $hA_{2A}$  AR model, the tricyclic core of **9** adopts the similar

	TM-I		TM-II				EL1				TM-III				EL2							
	1.35	1.39	2.57	2.60	2.61	2.62	2.64	2.65	2.66		3.28	3.29	3.32	3.33	3.36							
human A(2A)	Y9	E13	A59	F62	A63	I64	I66	S67	T68	G69	I80	A81	V84	L85	T88	A165	C166	L167	F168	E169	D170	V172
rat A(2A)	Y	E	A	F	A	I	I	S	T	G	F	A	V	L	T	T	C	L	F	E	D	V
human A(1)	Y	E	V	L	A	I	I	N	I	G	V	A	V	L	T	K	C	E	F	E	K	I
rat A(1)	Y	E	V	L	A	I	I	N	I	G	V	A	V	L	T	K	C	E	F	E	K	I

	TM-V		TM-VI				EL3				TM-VII											
	5.35	5.37	5.38	5.42	5.47	6.48	6.49	6.51	6.52	6.54	6.55	6.58		7.32	7.35	7.36	7.38	7.39	7.42	7.43		
human A(2A)	M174	Y176	M177	N181	V186	W246	L247	L249	H250	I252	N253	T256	H264	A265	P266	L267	M270	Y271	A273	I274	S277	H278
rat A(2A)	M	Y	M	N	V	W	L	L	H	I	N	T	H	A	P	P	M	Y	A	I	S	H
human A(1)	M	Y	M	N	V	W	L	L	H	L	N	T	H	K	P	S	T	Y	A	I	T	H
rat A(1)	M	Y	M	N	V	W	L	L	H	L	N	T	Q	K	P	S	I	Y	A	I	T	H

**Figure 3.** Alignment of  $hA_{2A}$ ,  $rA_{2A}$ ,  $hA_1$  and  $rA_1$  AR residues in the range of 5 Å from the ligands (according to the best docking poses of selected tricyclic purinediones at the homology models: (1)  $hA_{2A}$  AR + compd **9**, (2)  $rA_{2A}$  AR + compd **9**, (3)  $hA_1$  AR + compd **23**, (4)  $rA_1$  AR + compd **23**). Residue numbering for human  $A_{2A}$  AR sequence P29274, Ballesteros–Weinstein GPCR numbering given at the top). Residues situated farther than 5 Å from the docked ligand in the particular model are marked in brown.

location inside the binding pocket as the triazolotriazine system of ZM241385 in the 3EML X-ray structure (Fig. 4); the *N*3-ethyl substituent is buried in the same cavity as the furan ring of ZM241385. The purinedione scaffold of **9** is anchored by a hydrogen bond between the Asn253<sup>6.55</sup> and the carbonyl group in the 4-position (numbering according to the *hA*<sub>2A</sub> AR sequence P29274). Additionally, the flat heterocyclic core of **9** is involved in  $\pi$ - $\pi$  stacking with the conserved Phe168<sup>5.29</sup> (the extracellular loop 2, EL2) and in hydrophobic aliphatic contacts with Glu169<sup>5.30</sup> (EL2), Met177<sup>5.38</sup> and Leu85<sup>3.33</sup> from one side and Leu249<sup>6.51</sup> from the other side (Figs. 4 and 5). Almost identical location and analogous binding of the tricyclic scaffold of **9** can also be seen for the *rA*<sub>2A</sub> AR model (Fig. 5). According to the site-directed mutagenesis data for the *hA*<sub>2A</sub> AR, some of above-mentioned amino acids are important or even crucial for ligand binding. Replacement of Glu169<sup>5.30</sup>, His250<sup>6.52</sup>, Asn253<sup>6.55</sup>, Ile274<sup>7.39</sup> or His278<sup>7.43</sup> with alanine resulted in a total loss of XAC affinity at the *hA*<sub>2A</sub> AR, while mutation of Val84<sup>3.32</sup> decreased the affinity of antagonists. Recently published mutagenesis data also suggest, that conserved residues Phe168<sup>5.29</sup> and Leu249<sup>6.51</sup> play a central role in coordinating the bicyclic core present in both agonist and antagonist structures, while mutation of Met177<sup>5.38</sup> to alanine impeded antagonist binding.<sup>51,52</sup>

Small differences between docking poses of **9** at the human and rat *A*<sub>2A</sub> AR models are observed for the location of the hydroxyphenyl group (Fig. 5). In both cases the benzene ring of the ligand is situated near the extracellular region (the extracellular loops EL1 and EL2), close to the salt bridge between Glu<sup>5.30</sup> (EL2) and His<sup>6.66</sup> (EL3). In the *hA*<sub>2A</sub> AR binding site this aromatic function is placed in

proximity of the top TM-II, and the 4-hydroxy group of the ligand forms the hydrogen bond with Ile66<sup>2.64</sup>. In case of the rat model, the benzene ring is shifted towards the top of TM-VII and a hydrogen bond is formed between the 4-hydroxyl function of **9** and Tyr266<sup>7.36</sup> (residue numbering as for the *rA*<sub>2A</sub> AR sequence P30543<sup>50</sup>).

In this part of the binding site, small but significant structural differences can be observed for the human and rat *A*<sub>2A</sub> ARs sequences. In the *hA*<sub>2A</sub> AR Met<sup>7.35</sup> forms numerous hydrophobic contacts with the benzene ring of the ligand, while in the rat counterpart it is rotated and directed towards the fused pyrimidine ring of **9** (Fig. 5). Orientation of Met<sup>7.35</sup> seems to be at least partially triggered by the close presence of a residue in position 7.32 at the very top of helix TM-VII: a flexible Leu267 in the human *A*<sub>2A</sub> AR sequence is replaced with a rigid Pro262 in the *rA*<sub>2A</sub> AR. The difference in the 3D structure of this part of the binding site is reflected in the stronger van der Waals interactions between **9** and the individual residues of *rA*<sub>2A</sub> AR.

Apart from the mentioned Leu267/Pro262<sup>7.32</sup> exchange, in the range of 5 Å distance from the ligand **9**, there is only one more replacement in position 3.28: Ile80 in the *hA*<sub>2A</sub> AR is replaced by Phe77 in the *rA*<sub>2A</sub> AR. However, in both of our models, side chains of these residues seem to be too far away to have any important effect on affinity, and component terms of van der Waals interactions and Coulomb interactions energy, calculated for both residues, are small and insignificant.

Analysis of overall Glide energy terms, calculated for the final poses of **9** docked to the *hA*<sub>2A</sub> and the *rA*<sub>2A</sub> ARs models, showed similar values for the hydrogen bonding and van der Waals

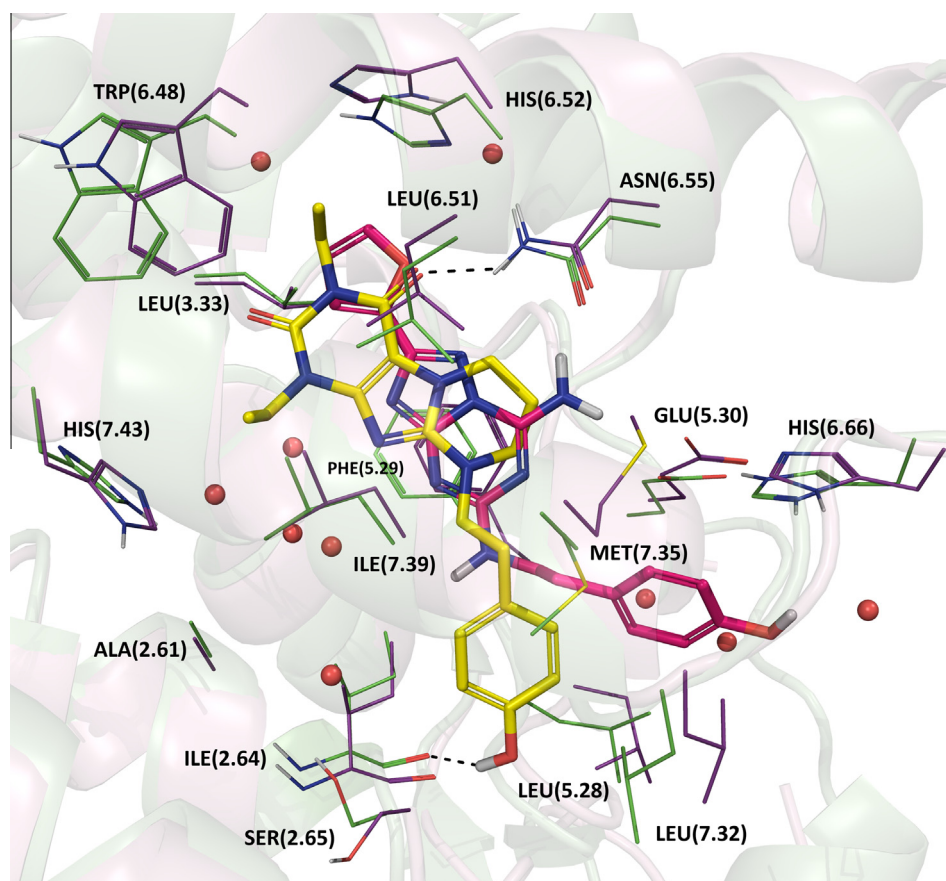


**Figure 4.** Superposition of 3EML X-ray structure and the *hA*<sub>2A</sub> AR model with the docked compound **9**. The ligands ZM241385 (pink) and the compound **9** (yellow) are shown in sticks. Selected residues of 3EML protein (purple) and the *hA*<sub>2A</sub> AR homology model (green) are shown in wires. For clarity only side chains are depicted (except Ile<sup>2.64</sup>). Residue numbering according to the Ballesteros–Weinstein GPCR numbering.

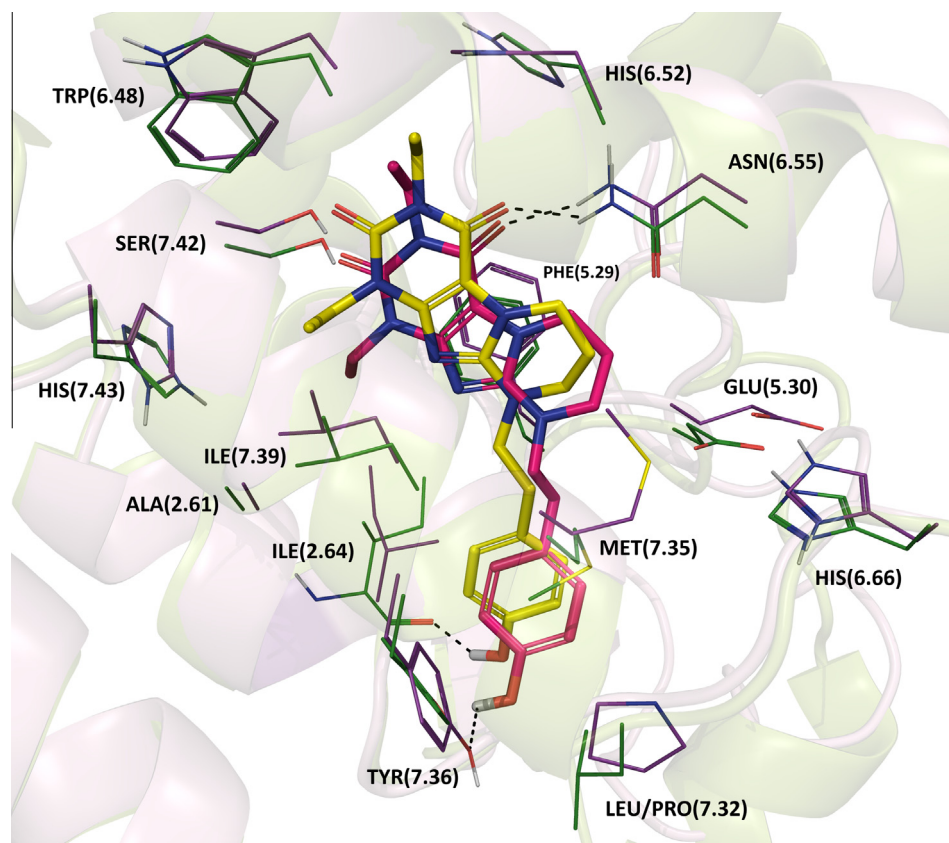


**Figure 5.** Superposition of the compound **9** docking poses in the human and rat  $A_{2A}$  AR models. The selected residues of the  $hA_{2A}$  model (green wires) and the  $rA_{2A}$  model (purple wires) are shown. The docking poses of the compound **9** are depicted in yellow sticks (docked to the  $hA_{2A}$  model) and pink sticks (docked to the  $rA_{2A}$  model). For clarity only side chains are depicted (except Ile<sup>2.64</sup>).

interactions. The electrostatic interactions, however, are more favorable in case of the rat  $A_{2A}$  AR model and this result significantly contributes to the higher docking score of **13** to the rat  $A_{2A}$  AR compared to the human counterpart.

#### 2.4.2. Binding mode of the xanthine **23** at the human and rat $A_1$ AR models

To compare the docking poses of the tricyclic xanthines and their interaction with the  $rA_1$  and the  $hA_1$  AR binding pockets, the example of the compound **23** was chosen for its highest affinity at the  $rA_1$  AR. In the docking pose observed for both,  $hA_1$  and  $rA_1$  AR models, **23** forms a hydrogen bond between Asn<sup>6.55</sup> and the carbonyl group in the 4-position (Fig. 6). The purinedione core of the ligand is involved in hydrophobic interactions with Phe<sup>5.29</sup> from one side and Leu<sup>6.51</sup>, Ile<sup>7.39</sup> and Asn<sup>6.55</sup> from the other side. The long butyl substituent in N3-position of the docked **23** occupies a similar cavity as the N3-ethyl chain of **13** in  $A_{2A}$  AR models, forcing a shift of the whole ligand tricyclic core towards the extracellular top of the receptor, compared to the position of **9**.

The benzene ring of **23** is stabilized by van der Waals interactions with surrounding residues of EL2 (Glu<sup>5.28</sup>, Glu<sup>5.30</sup>) as well as Tyr<sup>7.36</sup> and the residue in position 7.35. In both  $A_1$  AR models the side chains of the conserved Glu172/Glu172 in position 5.30 (numbering according to P30542 and P25099 for human and rat sequences, respectively<sup>50</sup>) forms single hydrophobic contacts and attractive electrostatic interactions with the ligand scaffold, but no H-bond is observed. The glutamate in position 5.28 (corresponding to leucine in  $hA_{2A}$  and  $rA_{2A}$  AR) adopts in  $A_1$  AR models two different conformations, but in both cases the carboxyl group of Glu<sup>5.28</sup> forms a salt bridge with the protonated amino group of **23** (Fig. 6).

In the obtained  $A_1$  AR models there are only two changes in the sequences within 5 Å distance from the docked ligand **23**. In TM-VII the residue Thr270<sup>7.35</sup> of the  $hA_1$  AR sequence corresponds to Ile270 in the  $rA_1$  AR (and Met270 in the  $hA_{2A}$  AR). Both side chains differ in lipophilicity, but in our models adopt a comparable position forming interactions with the ligand **23** in a similar way. Even though the hydroxyl group of threonine is not involved in any hydrogen bond with **23** in the observed docking poses, its direct proximity to the ligand scaffold might contribute to the species difference in the affinity of the compounds at the ARs.

Another structural difference is observed in the third extracellular loop EL3, where His264<sup>6.66</sup> in the  $hA_1$  AR corresponds to Gln264 in the  $rA_1$  AR (and His264 in  $hA_{2A}$  AR). In our  $hA_1$  AR model His264<sup>6.66</sup> does not form a salt bridge with Glu172<sup>5.30</sup> (EL2), as in case of  $A_{2A}$  AR models, but instead forms a hydrogen bond with the backbone carbonyl group of Thr257<sup>6.58</sup>, thereby stabilizing the position of the EL3. In the  $rA_1$  AR model the corresponding glutamine Gln264 plays a similar role, interacting by its side chain amide group with the backbone of Lys265<sup>6.67</sup> (EL3) from one side, and the hydroxyl group of Thr257<sup>6.58</sup> from the other side. At the same time Gln264 is placed 5 Å from the docking pose of **23** (acting by weak repulsive Coulomb forces), while in case of the  $hA_1$  AR model the distance of the docking pose of **23** from His264<sup>6.66</sup> is almost 7 Å (van der Waals and electrostatic interactions between them are negligible).

The proximity of Gln264<sup>6.66</sup> to  $rA_1$  AR-bound ligands (not necessarily xanthines) and the hydrogen bond feature of its side chain make this residue one of probable factors influencing the observed  $hA_1/rA_1$  AR selectivity. A putative ligand-Gln264<sup>6.66</sup> hydrogen bond might be formed directly or by means of the water network. A presence of water molecules in this part of the binding site was

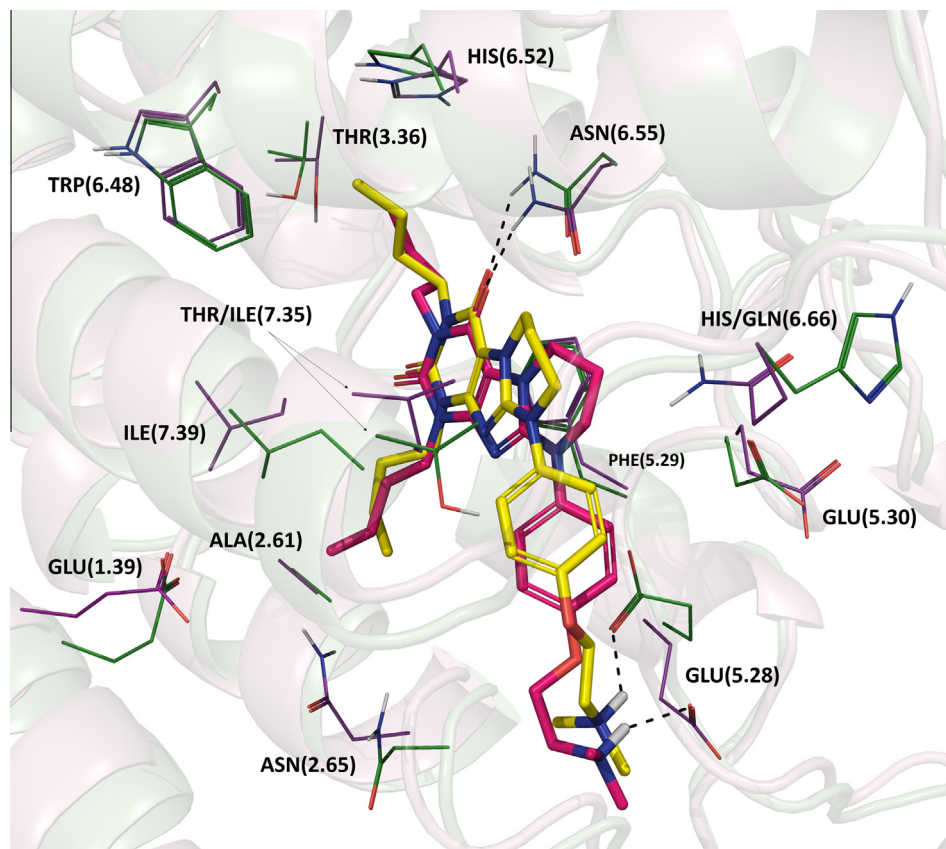


**Figure 6.** Superposition of the compound **23** docking poses in the human and rat  $A_1$  AR models. The selected residues of the  $hA_1$  model (green wires) and the  $rA_1$  model (purple wires) are shown. The docking poses of the compound **23** are depicted in yellow sticks (docked to the  $hA_1$  model) and pink sticks (docked to the  $rA_1$  model). For clarity only side chains are depicted.

described in case of 3EML crystal structure of the  $hA_{2A}$  AR, where in the direct vicinity of the His264<sup>6.66</sup> residue there is a water molecule involved in the hydrogen bond with the ligand ZM241385.

In terms of the stabilization energy, the compound **23** is better accommodated in the binding site of  $rA_1$  AR than  $hA_1$  AR. The higher docking score of **23** in  $rA_1$  AR is driven mainly by van der Waals energy, but also electrostatic interactions and hydrogen bonds terms contribute to this result. The better docking score is reflected in the higher affinity of **23** to this receptor compared to  $hA_1$  AR affinity.

#### 2.4.3. Comparison of the binding modes at the $rA_1$ and $rA_{2A}$ AR models

The analysis of binding sites in the rat  $A_1$  and  $A_{2A}$  AR models shows numerous differences in the sequences of both individual receptors (Figs. 3, 5 and 6). The most important mutations within the binding pocket of the subtypes  $rA_1$  and  $rA_{2A}$  are placed in proximity of the fused pyrimidine ring in the tricyclic core and in the proximity of the N9-aryl tail of the ligands, while the residues in the deep binding site, surrounding the purinedione scaffold, are highly conserved. This seems to indicate that the position, size and kind of substituent in the pyrimidine ring, interacting with the top part of the receptor, has a big influence on the subtype selectivity, while contacts of the purinedione system with the conserved transmembrane domains are responsible for the affinity to both subtypes.

In the range of 5 Å distance from the ligands **9** or **23**, the differences between the  $rA_1$  and  $rA_{2A}$  AR sequences are: Asn70/Ser64<sup>2.65</sup>, Ile71/Thr65<sup>2.66</sup>, Val83/Phe77<sup>3.28</sup>, Lys168/Thr160 (EL2), Glu170/Leu162 (EL2), Lys173/Asp165 (EL2), Leu253/Ile247<sup>6.54</sup>, Gln264/His259 (EL3), Lys265/Ala260 (EL3), Ser267/Pro262<sup>7.32</sup> and Ile270/

Met265<sup>7.35</sup>. One of the most important replacements is undoubtedly the exchange in position 5.28 of EL2, which, in all our homology models is in the direct proximity of the docked ligands **9** and **23**. In this position leucine, present in both rat and human  $A_{2A}$  AR sequence is exchanged into glutamate in  $A_1$  AR sequence. The energy contributions, calculated for interactions: compound **23**-Glu<sup>5.28</sup> in the  $A_1$  AR models and compound **9**-Leu<sup>5.28</sup> in the  $A_{2A}$  AR models show that the presence of glutamate is beneficial for the ligand binding. Apart from the hydrogen bond between the carboxyl function of Glu<sup>5.28</sup> and the charged amine group of the xanthine **23**, reflected in H-bond and electrostatic energy contributions, also van der Waals interactions between glutamate and the ligand are favorable, compared to leucine in this position.

Observed differences within the sequences are located to a large extent in the extracellular region, especially within the second and the third extracellular loop. Among adenosine receptors EL2 is described to be essential for receptor activation<sup>53–56</sup> and plays an important role in ligand recognition, binding and subtype selectivity,<sup>53,54</sup> while EL3 may be involved in receptor activation and binding of ligands.<sup>54,55</sup> However, due to their flexibility and high variability of sequences, loops are difficult subject of unambiguous prediction using the homology modeling method. The most problematic for mapping is the highly divergent EL2 region, containing 33 residues in the  $rA_1$  AR sequence and 31 residues in the  $rA_{2A}$  AR.<sup>43,44</sup> Moreover, the extracellular part of the receptor is exposed to water, often involved in H-bond network with the receptor and the ligand. Therefore, in most cases both the position and the influence of individual structural differences within the extracellular loops on the observed ligand affinity and selectivity is difficult to unambiguously estimate.

### 3. Conclusion

A new series of 32 tetrahydropyrimido- and 5 tetrahydropyrazino[2,1-*f*]purinediones was designed, synthesized and evaluated for their rat and human adenosine receptor affinities. Insertion of a basic amino group into the *N*9-substituent as well as the exchange of the fused pyrimidine ring to a pyrazine ring resulted in a significant increase in the calculated solubility of compounds, compared to the lead structures: 4-methoxyphenyl- or 4-methoxyphenylethyl-substituted derivatives of 1,3-dialkyl-6,7,8,9-tetrahydropyrimido-[1,2-*f*]purine-2,4(1*H*,3*H*)-diones. The increased water solubility of the *N*9-aryl and especially *N*9-arylethyl analogues was confirmed by the experimental assay performed for selected compounds.

In the group of the pyrimido derivatives most compounds showed measurable affinity at *rA*<sub>1</sub> and/or *rA*<sub>2A</sub> ARs, and among the 1,3-dibutyl derivatives possessing an amine group potent *rA*<sub>1</sub> AR antagonists were identified with *K*<sub>i</sub> values in the range of 56–80 nM. Affinity for *hA*<sub>2B</sub> and *hA*<sub>3</sub> ARs was shown mainly within the *N*9-arylethyl series, in particular for 1,3-dibutyl compounds with *K*<sub>i</sub> at *hA*<sub>2B</sub> AR in range of 109–337 nM.

Docking experiments of the investigated library to the homology models of the human and rat *A*<sub>1</sub> and *A*<sub>2A</sub> ARs allowed to compare the expected binding modes for selected tricyclic xanthines. Analysis of the binding site structures revealed a highly conserved protein region in close proximity of ligands, especially within the rat and the human orthologues of a particular receptor. The contributions to the overall interaction energies calculated for the individual residues show that single amino acid replacements found in the closest surroundings of the docking poses **9** and **23** (Leu267/Pro262<sup>7,32</sup> in case of *hA*<sub>1</sub>/*rA*<sub>1</sub> AR, Thr270/Ile270<sup>7,35</sup> and His264/Gln264<sup>6,66</sup> in case of *hA*<sub>2A</sub>/*rA*<sub>2A</sub> AR) may have a significant influence on the species selectivity, but in case of the investigated xanthines the observed 7–10 fold difference in the rat/human AR affinity is driven mainly by overall electrostatic and van der Waals interactions. More structural divergences can be found within the binding sites of the *A*<sub>1</sub> and the *A*<sub>2A</sub> AR subtypes, especially in the extracellular regions surrounding the *N*9-substituent. Among those differences the Glu/Leu<sup>5,28</sup> in EL2 seems to be the most significant one for ligand binding from an energy point of view.

### 4. Experimental protocols

#### 4.1. Chemistry

All reagents were purchased from commercial suppliers and were used without further purification. Melting points (mp.) were determined on a MEL-TEMP II (LD Inc., USA) melting point apparatus and are uncorrected. <sup>1</sup>H NMR spectra were recorded at 300 MHz using a Varian-Mercury-VX 300 MHz PFG spectrometer or a Bruker AMX 300 spectrometer (Bruker, Germany). Chemical shifts were expressed in parts per million (ppm). <sup>13</sup>C NMR spectra were recorded at 75 MHz on Varian-Mercury-VX 300 MHz PFG or 400 MHz spectrometer. IR spectra were measured as KBr pellets on FT/IR-410 Spectrometer (Jasco) or FT/IR Nicolet iS5 Spectrometer (ThermoScientific). UV spectra were recorded on Jasco UV/Vis V-530 spectrometer in a concentration of 10<sup>-2</sup> g/L or 10<sup>-3</sup> g/L in methanol. Mass spectra (LC/MS) were performed on Waters TQ Detector mass spectrometer coupled to a Waters Acquity Ultra Performance Liquid Chromatography (UPLC). The UPLC purity of all final compounds was determined (%). Elemental analyses (C, H, N) were performed on an Elemental Analyser Vario El III (Hanau, Germany). For column chromatography purification silica gel 60 (0.063–0.20 mm; Merck) was used and the mixture of dichloromethane with methanol was applied as a mobile phase.

The synthesis and physicochemical properties of the compounds **3a**, **3b**, **4** and **8** were reported previously.<sup>18,19</sup> Procedures, yields and physical data of the selected compounds are given below, for all other obtained xanthine derivatives the analytical data can be found in [Supplementary Data](#).

#### 4.1.1. General procedure for the synthesis of 4-(4-hydroxyphenyl)-4-(4-hydroxyphenylethyl) substituted derivatives of 1,3-dialkyl-6,7,8,9-tetrahydropyrimido-[1,2-*f*]purine-2,4(1*H*,3*H*)-diones (**4-11**)

A mixture of 2 mmol of 1,3-dialkyl-8-bromo-7-(3-chloropropyl)-xanthine and 4 mmol of commercial available 4-aminophenol or tyramine (obtained *ex tempore* from saturated aqueous solution of tyramine hydrochloride by alkalization with 25% Na<sub>2</sub>CO<sub>3</sub>) was refluxed in DMF for 5–10 h. Raw products were precipitated by addition of water to the reaction mixture, filtered off and purified by crystallization from ethanol.

#### 1,3-Diethyl-9-(4-hydroxyphenyl)-6,7,8,9-tetrahydropyrimido [1,2-*f*]purine-2,4(1*H*,3*H*)-dione (**5**)

The reaction was carried out for 8 h. The raw product was crystallized from ethanol. Yield: 76%; mp 238–240 °C. Anal. for C<sub>18</sub>H<sub>21</sub>N<sub>5</sub>O<sub>3</sub>: Calcd: C, 60.83; H, 6.96; N, 19.71. Found: C, 60.75; H, 6.68; N, 19.48; LC/MS: purity 100%, *m/z* 356.35 [M<sup>+</sup>+1]. <sup>1</sup>H NMR (CDCl<sub>3</sub>) δ: 1.02–1.15 (m, 6H, 2CH<sub>3</sub>CH<sub>2</sub>), 2.12–2.23 (m, 2H, CH<sub>2</sub>CH<sub>2</sub>CH<sub>2</sub>), 3.68 (t, *J* = 5.3 Hz, 2H, CH<sub>2</sub>CH<sub>2</sub>CH<sub>2</sub>), 3.77–3.91 (m, 4H, 2CH<sub>3</sub>CH<sub>2</sub>), 4.17 (t, *J* = 5.8 Hz, 2H, CH<sub>2</sub>CH<sub>2</sub>CH<sub>2</sub>), 6.75 (d, *J* = 8.7 Hz, 2H, Ar), 7.22 (d, *J* = 8.7 Hz, 2H, Ar), 9.42 (s, 1H, OH). <sup>13</sup>C NMR (CDCl<sub>3</sub>) δ: 13.1, 13.4, 21.6, 36.2, 38.6, 42.1, 49.1, 103.3, 116.7, 126.5, 134.9, 147.5, 150.7, 150.8, 153.9, 155.2. IR ν (cm<sup>-1</sup>): 3169 (OH), 1694 (C=O), 1650 (C=O); UV λ<sub>max</sub> (nm): 305.

#### 4.1.2. The synthesis of 8-(4-hydroxyphenethyl)-1,3-dimethyl-6,7,8,9-tetrahydropyrazino[2,1-*f*]purine-2,4(1*H*,3*H*)-dione (**38**)

A mixture of 2 mmol of 7-(2-chloroethyl)-8-(chloromethyl)-1,3-dimethyl-1*H*-purine-2,6(3*H*,7*H*)-dione and 4 mmol of tyramine (obtained *ex tempore* from saturated aqueous solution of tyramine hydrochloride by alkalization with 25% Na<sub>2</sub>CO<sub>3</sub>) was refluxed in DMF medium for 20 h. After cooling and addition of water the brown solid precipitated and was filtered off. A raw product was purified by crystallization from ethanol.

Yield: 63%; mp 259–261 °C. Anal. for C<sub>18</sub>H<sub>21</sub>N<sub>5</sub>O<sub>3</sub>×H<sub>2</sub>O: Calcd: C, 57.89; H, 6.21; N, 18.76. Found: C, 57.77; H, 6.29; N, 19.04. LC/MS: purity 100%, *m/z* 356.35 [M<sup>+</sup>+1]. <sup>1</sup>H NMR (CDCl<sub>3</sub>) δ: 2.47–2.52 (m, 4H, CH<sub>2</sub>CH<sub>2</sub>Ar), 2.92–3.00 (m, 2H, CH<sub>2</sub>CH<sub>2</sub>), 3.21 (s, 3H, N<sup>1</sup>CH<sub>3</sub>), 3.40 (s, 3H, N<sup>3</sup>CH<sub>3</sub>), 3.44–3.54 (m, 4H, CH<sub>2</sub>CH<sub>2</sub>+CH<sub>2</sub>), 4.68 (s, 1H, OH), 6.71 (d, *J* = 8.6 Hz, 2H, Ar), 7.09 (d, *J* = 8.6 Hz, 2H, Ar). <sup>13</sup>C NMR (CDCl<sub>3</sub>) δ: 27.9; 29.7, 32.8, 44.3, 54.0, 57.6, 59.3, 106.6, 114.7, 129.6, 131.6, 148.0, 148.5, 151.7, 157.3, 162.8. IR ν (cm<sup>-1</sup>): 3336 (OH), 1683 (C=O), 1624 (C=O); UV λ<sub>max</sub> (nm): 229.

#### 4.1.3. General procedure for the synthesis of 4-(2-aminoethoxy)phenyl and 4-(2-aminoethoxy)phenethyl derivatives of 1,3-dialkyl-6,7,8,9-tetrahydropyrimido- and 1,3-dimethyl-6,7,8,9-tetrahydropyrazino[1,2-*f*]purine-2,4(1*H*,3*H*)-diones (**12–37**, **39–42**)

A mixture of 2 mmol of:

9-(4-hydroxyphenyl)-1,3-dialkyl-6,7,8,9-tetrahydropyrimido- (**4-7**) or

9-(4-hydroxyphenethyl)-1,3-dialkyl-6,7,8,9-tetrahydropyrimido- (**8-11**) or

8-(4-hydroxyphenethyl)-1,3-dimethyl-6,7,8,9-tetrahydropyrazino[1,2-*f*]purine-2,4(1*H*,3*H*)-dione (**38**)

and the hydrochloride of the appropriate aminoethylchloride (dimethyl, diethyl, morpholine, pyrrolidine, piperidine) in 2 fold excess was refluxed in 2-butanone for 5–18 h, in the presence of  $K_2CO_3$  (4 mmol). The progress of the reaction was monitored by thin layer chromatography (TLC). The hot reaction mixture was filtered off to remove inorganic salts, cooled and concentrated in vacuo. The raw product was purified by crystallization or column chromatography (dichloromethane/methanol).

#### 9-(4-(2-(Diethylamino)ethoxy)phenyl)-1,3-dipropyl-6,7,8,9-tetrahydropyrimido[1,2-f]purine-2,4(1H,3H)-dione (19)

The reaction was carried out for 10 h. The raw product was crystallized from the mixture of ethanol and water. Yield: 71%; mp 94–96 °C. Anal. for  $C_{26}H_{38}N_6O_3$ : Calcd: C, 64.71; H, 7.94; N, 17.42. Found: C, 64.52; H, 7.91; N, 17.23; LC/MS: purity 98%,  $m/z$  483.59  $[M^+ + 1]$ .  $^1H$  NMR ( $CDCl_3$ )  $\delta$ : 0.82–0.97 (m, 6H,  $2CH_3CH_2CH_2$ ), 1.06 (t,  $J = 7.1$  Hz, 6H,  $2CH_2CH_3$ ), 1.57–1.76 (m, 4H,  $2CH_3CH_2$ ), 2.27 (quin,  $J = 5.7$  Hz, 2H,  $CH_2CH_2CH_2$ ), 2.64 (q,  $J = 7.0$  Hz, 4H,  $2CH_2CH_3$ ), 2.88 (t,  $J = 6.2$  Hz, 2H,  $OCH_2CH_2$ ), 3.76 (t,  $J = 5.5$  Hz, 2H,  $OCH_2CH_2$ ), 3.90 (q,  $J = 7.5$  Hz, 4H,  $2CH_2CH_2CH_3$ ), 4.05 (t,  $J = 6.3$  Hz, 2H,  $CH_2CH_2CH_2$ ), 4.32 (t,  $J = 6.0$  Hz, 2H,  $CH_2CH_2CH_2$ ), 6.89 (d,  $J = 9.0$  Hz, 2H, Ar), 7.30 (d,  $J = 9.0$  Hz, 2H, Ar).  $^{13}C$  NMR ( $CDCl_3$ )  $\delta$ : 47.8, 51.8, 66.7, 103.1, 114.7, 124.7, 136.3, 149.0, 149.9, 151.3, 154.1, 156.2. IR  $\nu$  ( $cm^{-1}$ ): 1693 (C=O), 1652 (C=O), 1245 (C–O); UV  $\lambda_{max}$  (nm): 305.

#### 1,3-Dibutyl-9-(4-(2-(dimethylamino)ethoxy)phenyl)-6,7,8,9-tetrahydropyrimido[1,2-f]purine-2,4(1H,3H)-dione (23)

The reaction was carried out for 10 h. The raw product was crystallized from the mixture of ethanol and water. Yield: 96%; mp 123–125 °C. Anal. for  $C_{26}H_{38}N_6O_3$ : Calcd: C, 64.71; H, 7.94; N, 17.42. Found: C, 63.36; H, 8.05; N, 17.24; LC/MS: purity 96%,  $m/z$  483.52  $[M^+ + 1]$ .  $^1H$  NMR ( $CDCl_3$ )  $\delta$ : 0.87–0.99 (m, 6H,  $2CH_3CH_2CH_2CH_2$ ), 1.25–1.45 (m, 4H,  $2CH_3CH_2CH_2CH_2$ ), 1.56–1.75 (m, 4H,  $2CH_3CH_2CH_2CH_2$ ), 2.23–2.31 (m, 2H,  $CH_2CH_2CH_2$ ), 2.34 (s, 6H,  $2CH_3$ ), 2.74 (t,  $J = 5.6$  Hz, 2H,  $OCH_2CH_2$ ), 3.79 (t,  $J = 5.5$  Hz, 2H,  $OCH_2CH_2$ ), 3.96 (q,  $J = 7.0$  Hz, 4H,  $2CH_3CH_2CH_2CH_2$ ), 4.08 (t,  $J = 5.6$  Hz, 2H,  $CH_2CH_2CH_2$ ), 4.34 (t,  $J = 5.9$  Hz, 2H,  $CH_2CH_2CH_2$ ), 6.92 (d,  $J = 9.0$  Hz, 2H, Ar), 7.33 (d,  $J = 9.0$  Hz, 2H, Ar).  $^{13}C$  NMR ( $CDCl_3$ )  $\delta$ : 42.9, 45.9, 47.8, 58.3, 66.2, 103.1, 111.8, 124.6, 136.3, 148.2, 149.9, 151.3, 154.0, 156.1. IR  $\nu$  ( $cm^{-1}$ ): 1697 (C=O), 1660 (C=O), 1249 (C–O); UV  $\lambda_{max}$  (nm): 306.

#### 9-(4-(2-(Diethylamino)ethoxy)phenylethyl)-1,3-dimethyl-6,7,8,9-tetrahydropyrimido[1,2-f]purine-2,4(1H,3H)-dione (29)

The reaction was carried out for 6 h. The raw product was crystallized from the mixture of ethanol and water. Yield: 59%; mp 150–152 °C. Anal. for  $C_{24}H_{34}N_6O_3$ : Calcd: C, 63.42; H, 7.54; N, 18.49. Found: C, 63.25; H, 7.67; N, 18.37; LC/MS: purity 98%,  $m/z$  455.40  $[M^+ + 1]$ .  $^1H$  NMR ( $CDCl_3$ )  $\delta$ : 1.07 (t,  $J = 7.2$  Hz, 6H,  $2CH_3$ ), 2.03 (quin,  $J = 5.8$  Hz, 2H,  $CH_2CH_2CH_2$ ), 2.64 (q,  $J = 6.9$  Hz, 4H,  $2CH_2CH_3$ ), 2.85–2.91 (m, 4H,  $OCH_2CH_2 + CH_2CH_2$ ), 3.18 (t,  $J = 5.5$  Hz, 2H,  $CH_2CH_2$ ), 3.37 (s, 3H,  $N^3CH_3$ ), 3.53 (s, 3H,  $N^1CH_3$ ), 3.70 (t,  $J = 7.3$  Hz, 2H,  $OCH_2CH_2$ ), 4.02 (t,  $J = 6.3$  Hz, 2H,  $CH_2CH_2CH_2$ ), 4.16 (t,  $J = 6.0$  Hz, 2H,  $CH_2CH_2CH_2$ ), 6.84 (d,  $J = 8.5$  Hz, 2H, Ar), 7.11 (d,  $J = 8.5$  Hz, 2H, Ar).  $^{13}C$  NMR ( $CDCl_3$ )  $\delta$ : 66.5, 102.8, 114.6, 129.7, 130.9, 149.2, 151.5, 151.9, 153.8, 157.5. IR  $\nu$  ( $cm^{-1}$ ): 1697 (C=O), 1649 (C=O), 1246 (C–O); UV  $\lambda_{max}$  (nm): 302.

#### 1,3-Dibutyl-9-(4-(2-(diethylamino)ethoxy)phenylethyl)-6,7,8,9-tetrahydropyrimido[1,2-f]purine-2,4(1H,3H)-dione (36)

The reaction was carried out for 11 h. The raw product was crystallized from the mixture of acetone and water. Yield: 31%; mp 72–74 °C. Anal. for  $C_{30}H_{46}N_6O_3$ : Calcd: C, 66.88; H, 8.63; N, 15.6. Found: C, 66.86; H, 8.57; N, 15.54; LC/MS: purity 99%,  $m/z$  539.26  $[M^+ + 1]$ .  $^1H$  NMR ( $CDCl_3$ )  $\delta$ : 0.88–1.03 (m, 6H,  $2CH_3CH_2CH_2CH_2$ ), 1.15 (br s, 6H,  $CH_3CH_2$ ), 1.32–1.47 (m, 4H,

$2CH_3CH_2CH_2CH_2$ ), 1.62 (quin,  $J = 7.5$  Hz, 2H,  $CH_3CH_2CH_2CH_2$ ), 1.74 (quin,  $J = 7.4$  Hz, 2H,  $CH_3CH_2CH_2CH_2$ ), 1.97–2.10 (m, 2H,  $CH_2CH_2CH_2$ ), 2.77 (br s, 4H,  $2CH_2CH_3$ ), 2.88 (t,  $J = 7.2$  Hz, 2H,  $CH_2CH_2$ ), 2.99 (br s, 2H,  $CH_2CH_2$ ), 3.19 (t,  $J = 5.5$  Hz, 2H,  $OCH_2CH_2$ ), 3.68 (t,  $J = 7.2$  Hz, 2H,  $OCH_2CH_2$ ), 3.96 (t,  $J = 7.0$  Hz, 2H,  $CH_2CH_2CH_2$ ), 4.05 (t,  $J = 7.2$  Hz, 2H,  $CH_2CH_2CH_2$ ), 4.09–4.23 (m, 4H,  $2CH_3CH_2CH_2CH_2$ ), 6.83 (d,  $J = 8.5$  Hz, 2H, Ar), 7.11 (d,  $J = 8.5$  Hz, 2H, Ar).  $^{13}C$  NMR ( $CDCl_3$ )  $\delta$ : 42.9, 44.5, 45.4, 47.8, 51.7, 66.4, 102.9, 114.6, 129.7, 131.0, 149.0, 151.3, 151.4, 153.8, 157.5. IR  $\nu$  ( $cm^{-1}$ ): 1698 (C=O), 1654 (C=O), 1247 (C–O); UV  $\lambda_{max}$  (nm): 302.

## 4.2. Pharmacology

### 4.2.1. Adenosine receptor binding assays

Adenosine receptor binding assays were performed as previously described<sup>31</sup> using rat brain cortical membrane preparations for  $A_1$  and rat brain striatal membrane preparations for  $A_{2A}$  AR assays. Frozen rat brains (unstripped) were obtained from Pel-Freez, Rogers, Arkansas, USA. For assays at human  $A_1$ ,  $A_{2A}$ ,  $A_{2B}$  and  $A_3$  ARs as well as at rat  $A_{2B}$  and  $A_3$  ARs, cell membranes of CHO cells expressing recombinant receptors were used as described.<sup>31</sup> The following compounds were used as radioligands:

$A_1$ : [ $^3H$ ]2-chloro- $N_6$ -cyclopentyladenosine ([ $^3H$ ]CCPA);  $A_{2A}$ : [ $^3H$ ]3-(3-hydroxypropyl)-7-methyl-8-( $m$ -methoxystyryl)-1-propargylxanthine ([ $^3H$ ]MSX-2);  $A_{2B}$ : [ $^3H$ ]4-(2-[7-amino-2-(2-furyl)-[1,2,4]-triazolo[2,3- $a$ ][1,3,5]triazin-5-ylamino]ethyl)phenol ([ $^3H$ ]ZM241385), or [ $^3H$ ]8-(4-(4-(4-chlorophenyl)piperazine-1-sulfonyl)phenyl)-1-propylxanthine ([ $^3H$ ]PSB-603), respectively;  $A_3$ : [ $^3H$ ]phenyl-8-ethyl-4-methyl-(8*R*)-4,5,7,8-tetrahydro-1*H*-imidazo[2,1- $i$ ]purine-5-one ([ $^3H$ ]PSB-11) and [ $^3H$ ]5'- $N$ -ethylcarboxamidoadenosine ([ $^3H$ ]NECA).

Initially, a single high concentration of compound was tested in three ( $A_1$ ,  $A_{2A}$ ) or two ( $A_{2B}$ ,  $A_3$ ) independent experiments. For potent compounds, full concentration-inhibition curves were determined using different concentrations of test compounds spanning at least 3 orders of magnitude. Data were analyzed using the PRISM program version 4.0 or higher (Graph Pad, San Diego, CA, USA).

### 4.2.2. Functional assays

cAMP accumulation experiments were essentially performed as previously described.<sup>31</sup> Stably transfected CHO cells expressing the human  $A_{2A}$  or  $A_{2B}$  receptor were grown in DMEM-F12 medium (Invitrogen) with 10% fetal calf serum, 100 U/ml penicillin G, 100 mg/ml streptomycin and 1% ultraglutamine at 37 °C with 5%  $CO_2$ . On the day of the experiment cells were transferred to 24-well plates at a density of 200,000 cells per well. After 24 h the medium was removed and the cells were washed with 500 ml of 37 °C warm Hank's Balanced Salt Solution (HBSS; 20 mM HEPES, 13 mM NaCl, 5.5 mM glucose, 5.4 mM KCl, 4.2 mM  $NaHCO_3$ , 1.25 mM  $CaCl_2$ , 1 mM  $MgCl_2$ , 0.8 mM  $MgSO_4$ , 0.44 mM  $KH_2PO_4$  and 0.34 mM  $Na_2HPO_4$ , pH adjusted to 7.3) containing 1 U/ml of adenosine deaminase (ADA, Sigma). The cells were then incubated in 300 ml of HBSS with ADA at 37 °C and 5%  $CO_2$  for 2 h. Then, the phosphodiesterase inhibitor Ro20-1724 (Hoffmann La Roche) was added to each well at a final concentration of 40  $\mu M$  and the cells were incubated for 15 min at 37 °C. Subsequently various dilutions of the agonist 5'- $N$ -ethylcarboxamidoadenosine (NECA, Sigma) in the presence or absence of a single concentration of test compound in HBSS containing 2.5% DMSO were added in duplicates. After 15 min of incubation at 37 °C the supernatant was removed and 500  $\mu l$  of 90 °C hot lysis buffer consisting of 4 mM EDTA and 0.01% Triton X-100 with the pH adjusted to 7.3 were added. After 1 h of mixing on ice, cAMP amounts in the cell lysates were determined by competitive radioligand binding experiments. cAMP competition experiments were performed in a final volume of

120 ml containing 50  $\mu$ l of cell lysates, 30  $\mu$ l of [ $^3$ H]cAMP solution in lysis buffer (final concentration 3 nM) and 40  $\mu$ l of cAMP binding protein diluted in the same buffer (50  $\mu$ g per sample). For determining cAMP concentrations 50  $\mu$ l of various cAMP concentrations were measured instead of cell lysates to obtain a standard curve. Total binding was determined by adding radioligand and binding protein to the lysis buffer, and the background was determined without addition of binding protein. The mixture was incubated for 60 min on ice and filtered through a GF/B glass fiber filter using a cell harvester (Brandel). The filters were washed three times, each with 2 ml of ice-cold 50 mM Tris–HCl buffer, pH 7.4, and subsequently transferred into scintillation vials. The liquid scintillation counting of the filters started after 9 h of incubation in 2.5 ml of scintillation cocktail (Lumag AG, Basel). Three separate experiments were performed. The amount of cAMP was determined by comparison to a standard curve generated for each experiment.

#### 4.3. Water solubility determination

Determination of the water solubility of selected compounds (**3a**, **3b**, **19**, **23**, **29** and **36**) was performed using UV spectroscopy on the basis of methods described earlier.<sup>35</sup> Saturated solutions of compounds (basic form) were prepared by suspending each compound (10 mg) in H<sub>2</sub>O (2 mL). The suspensions were mixed and boiled for 5 min, then left overnight at 20 °C and filtered off using filter *Macherey–Nagel MN 619 de*. Each filtrate was diluted in MeOH (from 10 to 80-fold) and analyzed by UV spectroscopy as a solution in MeOH/H<sub>2</sub>O (90%v/v). Standard curves were determined using known concentrations of each compound. Each stock solution was prepared (2 mg in 2 mL of the 90% MeOH) and further diluted to obtain seven different concentrations ranging from 10<sup>−3</sup> to 10<sup>−1</sup> mg/mL. The concentration of the saturated solutions for the compounds was determined by linear regression of two vicinal points from the standard curves and multiplication by the degree of dilution using *MS Excel*.

#### 4.4. X-ray structure analysis

In molecular docking calculations the knowledge on the 3D structure of tetrahydropyrimido- and tetrahydropyrazino[2,1-*f*]purinedione-based ligands adopted in the crystal state is useful. The library of tetrahydropyrimido[2,1-*f*]purinediones **4**–**37** was built, based on the reported crystallographic data for *N*9-phenyl- and *N*9-(2-benzyloxy)ethyl- derivatives.<sup>18,19</sup> Models of tetrahydropyrazino[2,1-*f*]purinediones were constructed using the 3D information obtained from the solved X-ray structures of **38** and **42** (Fig. 7).

#### 4.5. Molecular modeling

All models were downloaded from the Adenosiland website<sup>37</sup> and, together with the 3EML X-ray structure prepared to docking using the Protein Preparation Wizard option as a part of Schrödinger package.<sup>38</sup> In case of 3EML X-ray structure all non-protein atoms and the intracellular T4-lysozyme insertion were removed. The ligand binding cavity was confined to a box with 20 Å size. Docking studies for the reference adenosine receptor antagonists to the rigid receptor binding pocket were performed using Glide program,<sup>38</sup> with the standard precision (SP) mode. The amino hydrogen atom of the Asn<sup>655</sup> side chain in each models was used as a constrained H-bond donor for a ligand.

##### 4.5.1. Induced fit docking protocol

All the downloaded models were improved by induced fit docking procedure in Schrödinger Suite<sup>38</sup> using reference adenosine receptors antagonists (rolofylline and tonapofylline for *hA*<sub>1</sub>/*rA*<sub>1</sub>, istradefylline for *hA*<sub>2A</sub>/*rA*<sub>2A</sub>). In the initial step the side chains around the ligand were automatically trimmed (based on B-factor), then the side chains of the residues around 5 Å of ligand poses were refined using Prime application.

The stereochemical quality and compatibility of all final models was assessed by PROCHECK,<sup>39</sup> RAMPAGE<sup>40</sup> and ANOLEA.<sup>41</sup> Each 'improved' homology model together with the high-scored docking poses of the reference antagonists (rolofylline and tonapofylline for *hA*<sub>1</sub>/*rA*<sub>1</sub>, istradefylline for *hA*<sub>2A</sub>/*rA*<sub>2A</sub><sup>10,24</sup>) was additionally analyzed in Maestro program with respect to the model 3D structure, disulfide bonds (Table S1, Supplementary data) and binding cavity.

##### 4.5.2. Docking of tricyclic xanthine-based compounds

The 3D molecule models of tricyclic xanthines were built using Schrödinger Suite molecular modeling environment<sup>38</sup> based on the reported crystallographic data for *N*9-phenyl- and *N*9-(2-benzyloxy)ethyl derivatives. Models of tetrahydropyrazino[2,1-*f*]purinediones were constructed using the 3D information obtained from the solved X-ray structures of **38** and **42**. The ligands library was prepared with LigPrep module (low energy ionization/protonation state in pH = 7 ± 1, tautomeric state) optimized by conformational search (MacroModel). The geometry optimization was performed using the multiple minimization method as implemented in MacroModel 9.7 with MMFFs force field and Truncated Newton Conjugate Gradient (TNCG) options and terminated when the root means square (RMS) of conjugate gradient was below 0.05 kJ mol<sup>−1</sup> Å<sup>−1</sup>. The minimization was carried out in vacuum, with dielectric constant 1.0 as a way to treat electrostatic interactions.

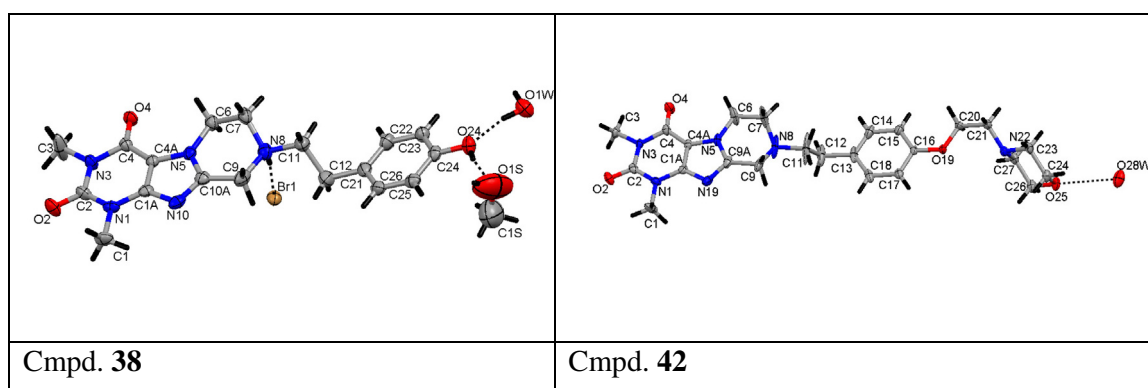


Figure 7. Crystal structures of tetrahydropyrazino[2,1-*f*]purinedione-based compounds **38** and **42**.

Docking simulations of low-energy conformations for all compounds were performed with SP mode to all improved homology models of adenosine receptors, with the constrained H-bond between the side chain amino group of Asn<sup>6.55</sup> and the ligand. Five poses obtained after docking for each ligand (RMS deviation higher than 0.5 Å) were post-minimized, and final poses were kept and analyzed according to the obtained docking score values.

The selected physicochemical properties, namely partition coefficient (QPlogP<sub>o/w</sub>) and water solubility (QPlogS) were evaluated using QikProp module.<sup>38</sup>

For the graphic presentation of the selected structures with the highest docking scores, representing individual clusters of poses, PyMOL software was used.<sup>57</sup>

## Acknowledgements

Financial support of this research by the National Science Centre Poland (DEC/2012/04/M/NZ4/00219) is gratefully acknowledged. C.E.M. is grateful for support by the Alzheimer Forschung Initiative (AFI) e.V.

## Supplementary data

Supplementary data associated with this article can be found, in the online version, at <http://dx.doi.org/10.1016/j.bmc.2016.07.028>.

## References and notes

- McKim, W. A.; Hancock, S. In *Drugs & Behavior: An Introduction to Behavioral Pharmacology*; Pearson, 2012; pp 209–227.
- Dillinger, T. L.; Barriga, P.; Escarcega, S.; Jimenez, M.; Lowe, D. S.; Grivetti, L. E. *J. Nutr.* **2000**, *130*, 2057S.
- Jacobson, K. A. In *Adenosine Receptors in Health and Disease*; Wilson, C. N., Mustafa, S. J., Eds.; Springer: Berlin Heidelberg, 2009; Vol. 193, pp 1–24.
- Francis, S. H.; Sekhar, K. R.; Ke, H.; Corbin, J. D. In *Methylxanthines*; Fredholm, B. B., Ed.; Springer: Berlin Heidelberg, 2011; Vol. 200, pp 93–134.
- Howell, L. L.; Coffin, V. L.; Speelman, R. D. *Psychopharmacology* **1997**, *129*, 1.
- Fredholm, B. B.; Ijzerman, A. P.; Jacobson, K. A. J. L.; Müller, C. E. *Pharmacol. Rev.* **2011**, *63*, 1.
- Chen, J. F.; Eltischig, H. K.; Fredholm, B. B. *Nat. Rev. Drug Disc.* **2013**, *12*, 265.
- Jacobson, K. A.; Müller, C. E. *Neuropharmacology* **2016**, *104*, 31.
- Sachdeva, S.; Gupta, M. *Saudi Pharm. J.* **2013**, *21*, 245.
- Müller, C. E.; Jacobson, K. A. *Biochim. Biophys. Acta* **2011**, *1808*, 1290.
- Biogen. Oral BG9928 in patients with heart failure and renal insufficiency, ClinicalTrials.gov [Internet]. Bethesda (MD): National Library of Medicine (US). 2000– [cited 2015 Aug 31]. Available from: <http://www.clinicaltrials.gov/ct2/show/NCT00745316> Identifier: NCT00745316.
- Madden, D. R.; Armstrong, N.; Svergun, D.; Perez, J.; Vachette, P. *J. Biol. Chem.* **2005**, *280*, 23637.
- Dungo, R.; Deeks, E. D. *Drugs* **2013**, *73*, 875.
- Preti, D.; Baraldi, P. G.; Moorman, A. R.; Borea, P. A.; Varani, K. *Med. Res. Rev.* **2015**, *35*, 790.
- Petzer, J. P.; Petzer, A. *Curr. Med. Chem.* **2015**, *22*, 975.
- Tarazi, F. I.; Sahli, Z. T.; Wolny, M.; Mousa, S. A. *Pharmacol. Ther.* **2014**, *144*, 123.
- Laurent, C.; Burnouf, S.; Ferry, B.; Batalha, V. L.; Coelho, J. E.; Baqi, Y.; Malik, E.; Marciniaik, E.; Parrot, S.; Van der Jeugd, A.; Faivre, E.; Flaten, V.; Ledent, C.; D'Hooge, R.; Sergeant, N.; Hamdane, M.; Humez, S.; Muller, C. E.; Lopes, L. V.; Buee, L.; Blum, D. *Mol. Psychiatry* **2016**, *21*, 97.
- Drabczyńska, A.; Müller, C. E.; Lacher, S. K.; Schumacher, B.; Karolak-Wojciechowska, J.; Nasal, A. P. K.; Yuzlenko, O.; Pękala, E.; Kieć-Kononowicz, K. *Bioorg. Med. Chem.* **2006**, *14*, 7258.
- Drabczyńska, A.; Müller, C. E.; Schiedel, A.; Schumacher, B.; Karolak-Wojciechowska, J.; Fruzinski, A.; Zobnina, W.; Yuzlenko, O.; Kieć-Kononowicz, K. *Bioorg. Med. Chem.* **2007**, *15*, 6956.
- Drabczyńska, A.; Müller, C. E.; Karolak-Wojciechowska, J.; Schumacher, B.; Schiedel, A.; Yuzlenko, O.; Kieć-Kononowicz, K. *Bioorg. Med. Chem.* **2007**, *15*, 5003.
- Drabczyńska, A.; Yuzlenko, O.; Köse, M.; Paskaleva, M.; Schiedel, A. C.; Karolak-Wojciechowska, J.; Handzlik, J.; Karcz, T.; Kuder, K.; Müller, C. E.; Kieć-Kononowicz, K. *Eur. J. Med. Chem.* **2011**, *46*, 3590.
- Drabczyńska, A.; Karcz, T.; Szymańska, E.; Kose, M.; Müller, C. E.; Paskaleva, M.; Karolak-Wojciechowska, J.; Handzlik, J.; Yuzlenko, O.; Kieć-Kononowicz, K. *Purinergic Signal.* **2013**, *9*, 395.
- Szymańska, E.; Mazurkiewicz, J.; Kieć-Kononowicz, K. *Heterocycl. Commun.* **2013**, *19*, 297.
- Müller, C. E.; Jacobson, K. A. In *Methylxanthines*; Fredholm, B. B., Ed.; Springer: Berlin Heidelberg, 2011; Vol. 200, pp 151–199.
- Kim, S. A.; Marshall, M. A.; Melman, N.; Kim, H. S.; Müller, C. E.; Linden, J.; Jacobson, K. A. *J. Med. Chem.* **2002**, *45*, 2131.
- Van der Walt, M. M.; Terre-Blanche, G.; Petzer, A.; Lourens, A. C. U.; Petzer, J. P. *Bioorg. Chem.* **2013**, *49*, 49.
- Brunschweiler, A.; Koch, P.; Schlenk, M.; Pineda, F.; Kuppers, P.; Hinz, S.; Kose, M.; Ullrich, S.; Hockemeyer, J.; Wiese, M.; Heer, J.; Müller, C. E. *ChemMedChem* **2014**, *9*, 1704.
- Rybar, A.; Antos, K. *Collect. Czech. Chem. Commun.* **1970**, *35*, 1415.
- Bergmann, F.; Dikstein, S. *J. Am. Chem. Soc.* **1955**, *77*, 691.
- Perrin, D. D. *Dissociation Constants of Organic Bases in Aqueous Solution*; Butterworths: London, 1972.
- Alnouri, M. W.; Jepards, S.; Casari, A.; Müller, C. E. *Purinergic Signal.* **2014**, *10*, 769.
- Schnell, D.; Strasser, A.; Seifert, R. *Biochem. Pharmacol.* **2010**, *80*, 1437.
- Soriano-Ursua, M. A.; Ocampo-Lopez, J. O.; Ocampo-Mendoza, K.; Trujillo-Ferrara, J. G.; Correa-Basurto, J. *Comput. Biol. Med.* **2011**, *41*, 537.
- Auchampach, J. A.; Kreckler, L. M.; Wan, T. C.; Maas, J. E.; van der Hoeven, D.; Gizewski, E.; Narayanan, J.; Maas, G. E. *J. Pharmacol. Exp. Ther.* **2009**, *329*, 2.
- Vollmann, K.; Qurishi, R.; Hockemeyer, J.; Müller, C. E. *Molecules* **2008**, *13*, 348.
- Jaakola, V. P.; Griffith, M. T.; Hanson, M. A.; Cherezov, V.; Chien, E. Y. T.; Lane, J. R.; Ijzerman, A. P.; Stevens, R. C. *Science* **2008**, *322*, 1211.
- Floris, M.; Sabbadin, D.; Medda, R.; Bulfone, A.; Moro, S. *Eur. J. Med. Chem.* **2012**, *58*, 248.
- Schrödinger, Maestro, version 9.3.5; LigPrep, version 2.5; QikProp, version 3.5; Glide, version 5.8; Prime, version 3.1; Induced Fit Docking, Schrödinger Suite 2012 update 2; Schrödinger: New York, NY, 2012.
- Laskowski, R. A.; MacArthur, M. W.; Moss, D. S.; Thornton, J. M. *J. Appl. Crystallogr.* **1993**, *26*, 283.
- Lovell, S. C.; Davis, I. W.; Arendall, W. B.; de Bakker, P. I. W.; Word, J. M.; Prisant, M. G.; Richardson, J. S.; Richardson, D. C. *Proteins: Struct., Funct., Bioinf.* **2003**, *50*, 437.
- Melo, F.; Feytmans, E. *J. Mol. Biol.* **1998**, *277*, 1141.
- Ballesteros, J. A.; Weinstein, H. *Methods Neurosci.* **1995**, *25*, 366.
- Isberg, V.; Mordalski, S.; Munk, C.; Rataj, K.; Harpsøe, K.; Hauser, A. S.; Vroiling, B.; Bojarski, A. J.; Vriend, G.; Gloriam, D. E. *Nucleic Acids Res.* **2016**, *44*, D356.
- Isberg, V.; Vroiling, B.; van der Kant, R.; Li, K.; Vriend, G.; Gloriam, D. *Nucleic Acids Res.* **2014**, *42*, D422.
- Piirainen, H.; Ashok, Y.; Nanekar, R. T.; Jaakola, V. P. *Biochim. Biophys. Acta, Biomembr.* **2011**, *1808*, 1233.
- Martinelli, A.; Ortore, G. *Methods Enzymol.* **2013**, *522*, 37.
- Dore, A. S.; Robertson, N.; Errey, J. C.; Ng, I. W.; Hollenstein, K.; Tehan, B.; Hurrell, E.; Bennett, K.; Congreve, M.; Magnani, F.; Tate, C. G.; Weir, M.; Marshall, F. H. *Structure* **2011**, *19*, 1283.
- Hino, T.; Arakawa, T.; Iwanari, H.; Yurugi-Kobayashi, T.; Ikeda-Suno, C.; Nakada-Nakura, Y.; Kusano-Arai, O.; Weyand, S.; Shimamura, T.; Nomura, N.; Cameron, A. D.; Kobayashi, T.; Hamakubo, T.; Iwata, S.; Murata, T. *Nature* **2012**, *482*, 237.
- Congreve, M.; Andrews, S. P.; Dore, A. S.; Hollenstein, K.; Hurrell, E.; Langmead, C. J.; Mason, J. S.; Ng, I. W.; Tehan, B.; Zhukov, A.; Weir, M.; Marshall, F. H. *J. Med. Chem.* **2012**, *55*, 1898.
- UniProt Consortium *Nucleic Acids Res.* **2015**, *43*, D204.
- Kim, S. K.; Gao, Z. G.; Van Rompaey, P.; Gross, A. S.; Chen, A.; Van Calenbergh, S.; Jacobson, K. A. *J. Med. Chem.* **2003**, *46*, 4847.
- Jaakola, V. P.; Lane, J. R.; Lin, J. Y.; Katritch, V.; Ijzerman, A. P.; Stevens, R. C. *J. Biol. Chem.* **2010**, *285*, 13032.
- Seibt, B. F.; Schiedel, A. C.; Thimm, D.; Hinz, S.; Sherbiny, F. F.; Müller, C. E. *Biochem. Pharmacol.* **2013**, *85*, 1317.
- Peeters, M. C.; van Westen, G. J.; Li, Q. *Trends Pharmacol. Sci.* **2011**, *32*, 35.
- Peeters, M. C.; Wisse, L. E.; Dinaj, A.; Vroiling, B.; Vriend, G.; Ijzerman, A. P. *Biochem. Pharmacol.* **2012**, *84*, 76.
- Peeters, M. C.; Li, Q.; van Westen, G. J.; Ijzerman, A. P. *Purinergic Signal.* **2012**, *8*, 23.
- Pymol, Open-Source PyMOL Molecular Graphics System v. 1.5.0.4. DeLano Scientific.